Quadrature-based moment methods for the population balance equation: an algorithm review

Dongyue Li, Zhipeng Li, Zhengming Gao*
State Key Laboratory of Chemical Resource Engineering, School of Chemical Engineering,
Beijing University of Chemical Technology, Beijing, China
Email: gaozm@mail.buct.edu.cn, li.dy@dyfluid.com

***Abstract*—The dispersed phase in multiphase flows can be modeled by the population balance model (PBM). A typical population balance equation (PBE) contains terms for spatial transport, loss/growth and breakage/coalescence source terms. The equation is therefore quite complex and difficult to solve analytically or numerically. The quadrature-based moment methods (QBMMs) are a class of methods that solve the PBE by converting the transport equation of the number density function (NDF) into moment transport equations. The unknown source terms are closed by Gaussian quadrature. Over the years, many QBMMs have been developed for different problems, such as the quadrature method of moments (QMOM), direct quadrature method of moments (DQMOM), extended quadrature method of moments (EQMOM), conditional quadrature method of moments (CQMOM), extended conditional quadrature method of moments (ECQMOM) and hyperbolic quadrature method of moments (HyQMOM). In this paper, we present a comprehensive algorithm review of these QBMMs. The mathematical equations for spatially homogeneous systems with first-order point processes and second-order point processes are derived in detail. The algorithms are further extended to the inhomogeneous system for multiphase flows, in which the computational fluid dynamics (CFD) can be coupled with the PBE. The physical limitations and the challenging numerical problems of these QBMMs are discussed. Possible solutions are also summarized.**

***Index Terms*—PBE; QBMM; Multiphase flow; CFD**

I. Introduction

The population balance model (PBM) can be used to describe the evolution of a population of particles by the number density function (NDF) for many different industrial processes, such as gas-liquid dispersions [1]–[14], liquid-liquid dispersions [15]–[28], gas-particle flows [29]–[37], [37]–[41], aerosol engineering [42]–[45], crystallization [46]–[54], reacting flows and combustions [55]–[62], soot formation [63]–[65], and sprays [66]–[72], to cite just a few. Analysis of the particulate system seeks to synthesize the behavior of the population of particles and its environment from the behavior of single particles in their local environments. Readers who are interested in the numerical aspects of the industrial processes that are listed above are referred to the latest works [73]–[76]. Among researchers, chemical engineers have put population balances to the most diverse use for multiphase flows [77].

However, due to the complex characteristics of the population balance equation (PBE), the analytical solution can be acquired only under a rigid assumption [78]–[81]. Different numerical methods were developed and applied to solve the PBE, such as the class method (CM) [54], [82]–[84], method of moments (MOM) [85]–[87], method of weighted residuals (MWR) [88]–[91], Monte-Carlo method [92]–[101], direct quadrature spanning tree (DQST) method [102], [103], Lattice Boltzmann method [50], and method of manufactured solutions (MMS) [80], [104], [105] and others [106]–[108]. Each can be further divided into sub-methods, such as the higher-order moment conserving method of classes (HMMC) [109] and cell averaged technique (CAT) method [110], [111] in the CM, and the Taylor-series expansion method of moment (TEMOM) [112]–[115], finite-size-domain complete set of trial functions method of moments (FCMOM) [116], [117] and moment projection method (MPM) [118], [119] in the MOM. Each method has disadvantages and advantages over the others. For example, the CM can provide information on the shape of the NDF. However, it requires many discretized sections to achieve desirable accuracy, which is highly computational-resource demanding [77]. The multivariate CM may require more than 10 thousand equations to be solved in certain cases and the algorithm is cumbersome [6], [120]. The MOM can predict the mean Sauter diameter as accurately as the CM, but the main drawback is that the NDF can not be predicted directly. However, the derivative methods that are based on the MOM are very popular due to their balance between accuracy and computational resource requirements, especially when the PBE is coupled with computational fluid dynamics (CFD). The derivative methods that are based on the MOM are shown in Table. 1. The algorithms that employ Gaussian quadrature to close the source terms are grouped into the so-called quadrature-based moment methods (QBMMs), which distinguish themselves from others by using the quadrature weights and abscissas to calculate the unclosed terms.

Hulburt and Kats [85] pioneered the work of developing the MOM to solve the PBE. The MOM solves the PBE by tracking the time dependence of just the lower-order moments of the NDF, as the lower-order moments are sufficient for the investigation of the industrial processes by engineers. This is the point where it differentiates from the CM, in which the NDF is discretized as sections and each section is transported according to it's own transport equation. The source terms in PBE are closed by expressing them in terms of the lower-order moments. Therefore, the moment equation system is closed and the computational resource requirement is dramatically decreased. However, moment closure in the MOM requires a rigid restriction on the mathematical form of the source term,

which becomes an obstacle for applying the MOM to realistic processes.

To eliminate the rigid restriction in the MOM, McGraw [121] developed the quadrature method of moments (QMOM) to solve the PBE for growth problems. In the QMOM, the moments of the NDF are approximated by the n-point Gaussian quadrature, and the NDF can be approximated by the abscissas with a delta function. The abscissas (nodes) and weights can be calculated from the moments by a moment inversion algorithm, e.g., the product-difference (PD) algorithm [122] or the wheeler algorithm [123]. It was shown by McGraw [121] that the growth term can be easily approximated by Gaussian quadrature and it does not need to comply with a specific mathematical form. Meanwhile, the prediction of the time evolution of m_0 to m_5 agrees well with the analytical solution, with a relative error of less than 0.2% [121]. The QMOM was then applied to the coagulation problem [124], and the breakage and coalescence problems [125], [126]. Due to the simplicity of the QMOM, it can be easily coupled with a CFD solver.

However, the QMOM is only applicable to univariate distributions due to the limitations of Gaussian quadrature. To overcome this problem, Wright et al. [140] proposed a direct-inversion method in the context of particle coalescence and sintering. This method is usually referred to as the multivariate QMOM or the Brute-force QMOM [73]. Yoon and McGraw [141] developed the Tensor-product QMOM in the context of aerosol modeling. Baldyga et al. [142] developed the Gaussian Cubature (GC) technique for crystallization, aggregation and sintering. Another method is the direct quadrature method of moments (DQMOM) which was developed by Marchisio and Fox [127]. The main feature of the DQMOM is that the primitive variables (weights and abscissas) are transported instead of the conservative variables (moments). Therefore, application of the moment inversion algorithm is not necessary after the weights and abscissas have been found. Moreover, extending the univariate DQMOM to the multivariate DQMOM is straightforward and it has been applied to different industrial processes [143]–[147].

One of the biggest drawbacks of the DQMOM is that it is affected by problems that are related to the proper conservation of some moments of the NDF when it is coupled with CFD. These problems were prevented by the fully conservative DQMOM algorithm [6]. When the DQMOM is applied to purely hyperbolic transport equations, it will fail if there are shocks in the abscissas due to the discontinuity. This situation occurs most commonly when the velocity is the internal coordinate. For such cases, only the multivariate moment method appears to be able to overcome these problems. Thus, the CQMOM [120], [128] was proposed for solving the multivariate system efficiently and accurately. It employs conditional probability function theory to approximate the multivariate NDF. The conservative variables (the mixed moments) are transported and it is more robust than the DQMOM for problems in which shocks may occur (e.g., the gas velocity can be discontinuous in the Euler equation).

All the QBMMs that were discussed above only predict a discontinuous NDF, which will lead to problems in some cases. For example, if the PBE is used to simulate evaporation problems, a term that explains the loss of particles of zero size appears in the zero-order moment equation. To evaluate this term, the value of the NDF for a zero-size particle is required. If the QBMM was employed in large eddy simulation (LES) framework, the velocity dispersion around the velocity abscissa needs to be captured [148]. One possible solution is to increase substantially the number of abscissas so that the phase space is adequately discretized. However, the moment inversion algorithm is not accurate for N larger than approximately 10 [73]. The QBMMs that were discussed above will fall due to the discontinuous NDF reconstruction. To predict the continuous NDF, the EQMOM [129], [148] was developed. It can be viewed as an enhanced version of the QMOM, which employs an existing kernel density function (KDF) to approximate the NDF. After the moment transport equations have been solved, the parameters of the KDF can be calculated and a continuous NDF can be reconstructed. To calculate the additional unknown variance σ in the KDF, one additional moment transport equation is necessary. At last, it should be noted here that the hyperbolic quadrature method of moments (HyQMOM) was developed recently to circumvent the known disadvantages of the CQMOM when it was applied to KE [132] to prevent weak-hyperbolicity. It can be also combined with the CQMOM for problems with multivariate NDF and a CHyQMOM was constructed.

It can be seen that a large variety of QBMMs have been developed in past works to solve the PBE with univariate NDF or multivariate NDF. When the method is coupled with CFD for inhomogeneous multiphase systems, special numerical treatments need to be applied to ensure robustness and stability. The focus of this paper is to present an algorithm review for these methods. The advantages and drawbacks of each QBMM are reviewed in depth and summarized. The remainder of the work is organized as follows. In section 2 the algorithm of the QMOM, DQMOM, EQMOM, CQMOM and ECQMOM for spatially homogeneous systems is described. In section 3 the CFD-PBE coupling algorithm for spatially inhomogeneous multiphase systems is discussed. In section 4 the numerical aspects of the spatially transported moments, such as the boundedness problem, higher-order advection schemes, realizability of the moments, and reconstructed continuous NDF are investigated. Finally, conclusions are drawn in section 5.

II. Algorithms for spatially homogeneous systems

This NDF transport equation in the PBM can be given by different names. The *population balance equation* (PBE) is usually used to describe the evolution of the NDF, namely, $n(t, \mathbf{x}, \xi)$, which is independent of the velocity but dependent on an internal coordinate vector ξ, which can be the particle size d or the composition ϕ. The *kinetic equation* (KE) is usually used to describe the evolution of the velcocity number

TABLE I: Summary of the moment-based algorithms in the literature.

1st level derivatives	2nd level derivatives
QBMM	QMOM [121], DQMOM [127], DQMOM-FC [6], CQMOM [128], EQMOM [129], ECQMOM [73], Cumulative QMOM [130], ADQMOM [131], HQMOM [132], CHyQMOM [132]
SQMOM [133]	OPOSPM [134], MPSPM [135], SM-SQMOM [25]
FCMOM [116]	
TEMOM [112]	DEMM [136], GTEMOM [137]
MOMIC [138]	
$S-\gamma$ model [139]	
MPM [118]	

function (VDF), namely, $n(t, \mathbf{x}, \mathbf{U}_{\mathrm{d}})$, in which different velocities of the particles are considered. The KE is also called the Williams-Boltzmann equation in the field of sprays [149] and the general particle-dynamic equation in the field of aerosols [150]. When the NDF is dependent on both the velocity and other mesoscale variables (e.g., particle size), the governing equation for the NDF (e.g., $n(t, \mathbf{x}, \xi, \mathbf{U}_{\mathrm{d}})$) is usually called the *generalized population balance equation* (GPBE). In this work, we focus on the algorithms of the QBMMs for the PBE in spatially homogeneous and inhomogeneous systems. Unless otherwise stated, the internal coordinate is the particle size.

Consider a single computational volume, as shown in Fig.1. The NDF describes the number concentration of particles with sizes between d and $d+\mathrm{d}d$. Particles can break up into smaller particles or coalesce with other particles to form larger particles due to movement or external forces. The PBE describes the time evolution of the NDF. According to Fig.1, the unknown NDF is a distribution function instead of a vector value or a scalar value (e.g., $\mathbf{U}$ or p). The following PBE governs the evolution of the NDF:

$$\frac{\partial n(t,\mathbf{x},\xi)}{\partial t}+\nabla_{\mathbf{x}}\cdot(\mathbf{U}_{\mathrm{d}}n(t,\mathbf{x},\xi))+\nabla_{\xi}\cdot(\xi n(t,\mathbf{x},\xi))=S, \quad (1)$$

where $n(t, \mathbf{x}, \xi)$ is the NDF; $\mathbf{x}$ is the location vector, which is often referred to as the external coordinate; ξ is the internal coordinate vector; $\mathbf{U}_{\mathrm{d}}$ is the particle's velocity, which is assumed to be known in the PBE; S is the possible source term which is often called point processes in the field of PBM [73]; $\nabla_{\mathbf{x}}$ and ∇_{ξ} are divergence operators in the physical and phase spaces, respectively. Eq. (2) can be simplified further for different problems. For example, if only the particle size is included in the internal coordinate and continuous changes of particle size (the zero-point processes) can be neglected, Eq. (2) can be written as

$$\frac{\partial n(d)}{\partial t}=S \quad (2)$$

for a homogeneous system and

$$\frac{\partial n(d)}{\partial t}+\nabla\cdot(\mathbf{U}_{\mathrm{d}}n(d))=S \quad (3)$$

for an inhomogeneous system (the dependences of $n(t, \mathbf{x}, \xi)$ on t and $\mathbf{x}$ are omitted for simplicity). In Eq. (3), $\mathbf{U}_{\mathrm{d}}$ is often calculated by a CFD model. Nevertheless, after the simplification, the exact solution of Eq. (2) can be only acquired with rigid assumptions on the non-linear source terms. In the following, different solving methods for a homogeneous system are studied in details.

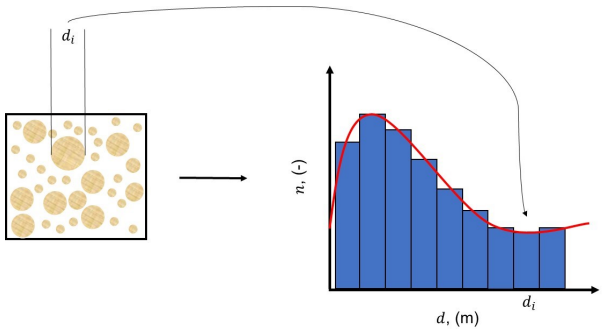

Fig. 1: An example of the NDF in one computational volume.

A. MOM

Although the MOM does not belong to the QBMMs since it is not based on the Gaussian quadrature closure, it is still necessary to discuss it here because it was the work of Hulburt and Katz [85] in which the NDF transport equation was first transformed into the moment transport equations. In the MOM, the k-th order moment of the NDF is defined by the following equations:

$$m_k=\int_0^{\infty}d^k n(d)\mathrm{d}d. \quad (4)$$

The lower-order moments may have specific physical meanings. For example, m_0 represents the total particle number per unit volume, m_2 is related to the total particle area per unit volume ($k_a m_2$, k_a is the surface shape factor), and m_3 is related to the total particle volume per unit volume ($k_v m_3$, k_v is the volume shape factor). The shape factors depend on particle morphology. The mean particle size can be defined as the ratio m_{k+1}/m_k for any value of k. It should be noted that the dimension of the NDF varies. Readers are suggested to the Appendix for further information. Usually, the mean Sauter diameter is used, which is defined by m_3/m_2. If we multiply the L.H.S. side of Eq. (2) by d^k and integrate it over d, the NDF transport equation is transformed into moment transport equations:

$$\int_0^{\infty}d^k\frac{\partial n}{\partial t}\mathrm{d}d=\frac{\partial m_k}{\partial t}=\int_0^{\infty}d^k S\mathrm{d}d. \quad (5)$$

Eq. (5) is not closed since the source terms include the unknown functions. The MOM imposes rigid constraint on the source terms to approximate them by the moments. Consider a typical zero-order-process, the growth source term can be written as the following equation:

$$S = -\frac{\partial Gn}{\partial d}, \tag{6}$$

where G is the growth function. If we multiply the R.H.S. of Eq. (6) by d^k and integrate over d, it can be simplified by the following relationship:

$$\begin{aligned} -\int_0^\infty \frac{\partial Gn}{\partial d} d^k \mathrm{d}d &= -\int_0^\infty d^k \mathrm{d}\left(Gn\right) \\ &= -d^k Gn \mid_0^\infty + k\int_0^\infty Gnd^{k-1}\mathrm{d}d \\ &= k\int_0^\infty Gnd^{k-1}\mathrm{d}d. \end{aligned} \tag{7}$$

In Eq. (7), $d^k Gn \mid_0^\infty$ equals zero since the tails of the NDF function tend to zero. By substituting Eq. (7) into Eq. (5), the moment transport equations with the growth source term can be written as:

$$\frac{\partial m_k}{\partial t} = k\int_0^\infty Gnd^{k-1}\mathrm{d}d. \tag{8}$$

Eq. (8) is not closed either because its R.H.S. depends on the unknown NDF. However, as reported in the work of Hulburt and Katz [85], if the growth term has a special shape, such as $\phi = G/d$, where G is a constant value, Eq. (8) can be written as follows:

$$\frac{\partial m_k}{\partial t} = kG\int_0^\infty nd^{k-2}\mathrm{d}d = kGm_{k-2}. \tag{9}$$

For simplicity, but without loss of generality, Eq. (9) can be expanded to the following set of moment equations:

$$\begin{aligned} \frac{\partial m_0}{\partial t} &= 0, \\ \frac{\partial m_1}{\partial t} &= Gm_{-1}, \\ \frac{\partial m_2}{\partial t} &= Gm_0, \\ \frac{\partial m_3}{\partial t} &= Gm_1. \end{aligned} \tag{10}$$

The systems in Eq. (10) has four equations with five unknown variables. Hulburt and Katz [85] further assumed that the NDF had a special mathematical form that was parametrized by its moments. For example, based on the Gamma distribution, the NDF can be expressed by the leading terms of the Laguerre series expansion. By this assumption, m_{-1} can be calculated by [85]

$$m_{-1} = \frac{m_0^2 m_1}{2m_1^2 - m_0 m_2}. \tag{11}$$

By substituting Eq. (11) into Eq. (10), the equation system is closed.

In the MOM, the moment equation system is self-closed by imposing a rigid restriction on the source term and the NDF. However, in contrast to the CM, only four moment transport equations need to be solved. One may ask whether other possible source terms, such as breakage and coalescence terms, can be treated in a similar way to form a self-closed equation system. Unfortunately, to the best of the author's knowledge, this is impossible due to their highly non-linear characteristics. This limits the ability to apply the MOM to realistic industrial processes. However, the MOM successfully transforms the NDF transport equation to moment transport equations, which constitute the fundamental basis of other QBMMs.

B. QMOM

The main strategy of the QMOM [121] is to approximate the tedious integrals that appear in the source terms by the n-point Gaussian quadrature. Mathematically, the Gaussian quadrature seeks to solve the integral numerically. For any given integral, it can be approximated by the following equation:

$$\int_\Omega f(x)\mathrm{d}x \approx \sum_{i=1}^N w_i f(x_i), \tag{12}$$

where w_i are the weights, x_i are the abscissas, and N is the number of weights (which is equal to the number of abscissas). The Gaussian quadrature calculates the integral by N's weights and abscissas of order $2N-1$. The essence of the quadrature-based closure is that the abscissas and weights can be completely specified in terms of the lower-order moments of the unknown NDF. For example, the k-th order moments can be computed by

$$m_k = \int_0^\infty d^k n(d)\mathrm{d}d = \sum_{i=1}^N d_i^k w_i. \tag{13}$$

Eq. (13) can be written in the following expanded form ($N = 2$):

$$\begin{aligned} w_1 + w_2 &= m_0, \\ d_1 w_1 + d_2 w_2 &= m_1, \\ d_1^2 w_1 + d_2^2 w_2 &= m_2, \\ d_1^3 w_1 + d_2^3 w_2 &= m_3, \end{aligned} \tag{14}$$

For any given initial moments m_k that correspond to a real NDF, Eq. (14) can be used to calculate the abscissas and weights. The direct solution to Eq. (14) requires a non-linear solver, such as the Newton-Raphson method [151]. McGraw [121] proposed to use the product-difference (PD) algorithm [122] to find the abscissas and weights, where abscissa i and weight i correspond to the eigenvalue and the first component of the ith eigenvector of the constructed tridiagonal matrix, respectively. The PD algorithm, or another similar algorithm (the Wheeler algorithm [123]), is usually called the *moment inversion algorithm* in the field of PBM. After the abscissas and weights have been calculated by the moment inversion algorithm, the source terms can be calculated and the equation system is closed. In the following, the breakage (first-order point process) and coalescence (second-order point process)

source terms are included in the moment transported equations as an example to demonstrate how the moment transport equations are closed in the QMOM.

The breakage and coalescence source terms are defined by [77]

$$\begin{aligned} & S(d) \\ & = \frac{d^2}{2} \int_0^d \frac{a\left(\left(d^3-d'^3\right)^{\frac{1}{3}}, d'\right)}{\left(d^3-d'^3\right)^{\frac{2}{3}}} n\left(\left(d^3-d'^3\right)^{\frac{1}{3}}\right) n(d') \, \mathrm{d}d' \\ & - n(d) \int_0^\infty a(d, d') n(d') \, \mathrm{d}d' + \int_d^\infty g\left(d'\right) \beta\left(d \mid d'\right) n\left(d'\right) \, \mathrm{d}d' \\ & - g(d) \, n(d), \end{aligned} \quad (15)$$

where $a(d, d')$ is the coalescence kernel, which quantifies the rate of coalescence of particles of size d (daughter particle) and d' (mother particle); $g(d)$ is the breakage kernel, which quantifies the frequency of breakage of particles of diameter d; and $\beta\left(d \mid d'\right)$ is the daughter size distribution function, which describes the number and size of particles that are formed by a breakage event. The first and second terms in the R.H.S. of Eq. (15) represent birth and death due to coalescence; the third and fourth terms in the L.H.S. of Eq. (15) represent birth and death due to breakage.

With the Gaussian quadrature, the death term and the birth term of the breakage source term can be calculated by

$$\int_0^\infty d^k g\left(d\right) n\left(d\right) \mathrm{d}d = \sum_{i=1}^N d_i^k g(d_i) w_i \quad (16)$$

and

$$\begin{aligned} & \int_0^\infty d^k \left(\int_d^\infty g\left(d'\right) \beta\left(d \mid d'\right) n\left(d'\right) \, \mathrm{d}d' \right) \mathrm{d}d \\ & = \int_0^\infty n\left(d'\right) g\left(d'\right) \left(\int_0^{d'} \beta\left(d \mid d'\right) d^k \, \mathrm{d}d \right) \mathrm{d}d' \\ & = \sum_{i=1}^N w_i g(d_i) \left(\int_0^{d_i} \beta\left(d \mid d_i\right) d^k \, \mathrm{d}d \right). \end{aligned} \quad (17)$$

For a given shape of the daughter size distribution function, e.g., $\beta\left(d \mid d_i\right) = 2/d_i$, an solution can be derived:

$$\int_0^{d_i} \beta\left(d \mid d_i\right) d^k \mathrm{d}d = \int_0^{d_i} \frac{2}{d_i} d^k \mathrm{d}d = \frac{2}{k+1} d_i^k. \quad (18)$$

By substituting Eq. (18) into Eq. (17), the birth term of the breakage becomes

$$\begin{aligned} & \int_0^\infty d^k \left(\int_d^\infty g\left(d'\right) \beta\left(d \mid d'\right) n\left(d'\right) \, \mathrm{d}d' \right) \mathrm{d}d \\ & = \frac{2}{k+1} \sum_{i=1}^N w_i g(d_i) d_i^k. \end{aligned} \quad (19)$$

Similarly, the death term and the birth term of the coalescence can be calculated by

$$\begin{aligned} & \int_0^\infty d^k \left(n(d) \int_0^\infty a(d, d') n(d') \, \mathrm{d}d' \right) \mathrm{d}d \\ & = \int_0^\infty d^k n(d) \left(\int_0^\infty a(d, d') n(d') \, \mathrm{d}d' \right) \mathrm{d}d \\ & = \sum_{i=1}^N w_i d_i^k \left(\int_0^\infty a(d_i, d') n(d') \, \mathrm{d}d' \right) \\ & = \sum_{i=1}^N w_i d_i^k \left(\sum_{j=1}^N a(d_i, d_j) w_j \right) \end{aligned} \quad (20)$$

and

$$\begin{aligned} & \int_0^\infty d^k \left(\frac{d^2}{2} \int_0^d \frac{a\left(\left(d^3-d'^3\right)^{\frac{1}{3}}, d'\right)}{\left(d^3-d'^3\right)^{\frac{2}{3}}} \right. \\ & \qquad \left. n\left(\left(d^3-d'^3\right)^{\frac{1}{3}}\right) n(d') \, \mathrm{d}d' \right) \mathrm{d}d \\ & = \int_0^\infty \left(u^3+d'^3\right)^{\frac{k}{3}} \left(\frac{d^2}{2} \int_0^\infty \frac{a\left(u, d'\right)}{u^2} n\left(u\right) n(d') \, \mathrm{d}d' \right) \frac{u^2}{d^2} \mathrm{d}u \\ & = \frac{1}{2} \int_0^\infty \left(u^3+d'^3\right)^{\frac{k}{3}} \left(\int_0^\infty a\left(u, d'\right) n\left(u\right) n(d') \, \mathrm{d}d' \right) \mathrm{d}u \\ & = \frac{1}{2} \int_0^\infty n(u) \left(\int_0^\infty a\left(u, d'\right) \left(u^3+d'^3\right)^{\frac{k}{3}} n(d') \, \mathrm{d}d' \right) \mathrm{d}u \\ & = \frac{1}{2} \sum_{i=1}^N w_i \left(\sum_{j=1}^N a(d_i, d_j) \left(d_i^3+d_j^3\right)^{\frac{k}{3}} w_j \right). \end{aligned} \quad (21)$$

where $u^3 = d^3 - d'^3$. By substituting Eq. (16), Eq. (19), Eq. (20), Eq. (21) and Eq. (15) into Eq. (5), the moment transport equations for the QMOM with breakage and coalescence source terms can be written as follows:

$$\begin{aligned} \frac{\partial m_k}{\partial t} = & \frac{1}{2} \sum_{i=1}^N w_i \left(\sum_{j=1}^N a(d_i, d_j) \left(d_i^3+d_j^3\right)^{\frac{k}{3}} w_j \right) \\ & - \sum_{i=1}^N w_i d_i^k \left(\sum_{j=1}^N a(d_i, d_j) w_j \right) \\ & + \sum_{i=1}^N w_i g(d_i) \left(\int_0^{d_i} \beta\left(d \mid d_i\right) d^k \, \mathrm{d}d \right) - \sum_{i=1}^N d_i^k g(d_i) w_i. \end{aligned} \quad (22)$$

After the weights and abscissas are calculated by the moment inversion algorithm from the given initial moments, Eq. (22) can be solved for the moments for the next time step. In the QMOM, the integrals in the source terms are transformed to summation operations by Gaussian quadrature. If $N = 3$,

only 6 moment transport equations need to be solved, which requires a total of $9+9+9+3=32$ summation operations.

The solution procedure of the QMOM is summarized as follows:

1) From the given initial moments, calculate the weights and abscissas by the moment inversion algorithm (e.g., PD algorithm).
2) Calculate the source term as reported in Eq. (22).
3) Calculate the unknown time derivatives of the moments in Eq. (22).
4) The iterative procedure is repeated from step 1.

The QMOM does not provide the information of the NDF directly since it only tracks its moments. The abscissas and weights have no exact physical meaning because they are only parts of the quadrature approximation. Nevertheless, they can be viewed as an approximation of the real NDF, as reported in Fig.2. Under such assumption, the NDF can be reconstructed by a sum of N delta functions, where each delta function represents a class of particles. Therefore, the NDF can be approximated by

$$n(d)=\sum_{i=1}^{N} w_i\delta(d-d_i). \tag{23}$$

The abscissas represent the particle sizes and the weights are their relative volume fractions. Eq. (23) is quite similar to the mathematical definition in the CM in which the NDF is defined by [152]

$$n(d)=\sum_{i=1}^{N} N_i\delta(d-d_i). \tag{24}$$

where N_i is the number of particles with diameter d_i. The main difference between the QMOM and the CM is that in the CM, the discrete particles need to be defined a-priori, which may introduce some problems when the engineer does not have information on the particle size interval. The only solution is to discretize the particle size over a large enough range to include all possible sizes. However, it forms many transport equations. In contrast, only few abscissas (e.g., $N=3$) are necessary in the QMOM and they move along the phase space axis flexibly. Meanwhile, they change their volume fractions (weights) to minimize the committed error.

Compared with other QBMMs, the QMOM is the simplest, and all the other algorithms that are discussed in the following are derived from the main concept of the QMOM. Due to its simplicity and robustness, the QMOM was employed to simulate a large variety of applications, such as gas-liquid dispersions [5], [153], liquid-liquid dispersions [21], gas-particle flows [32], pipe flows [154], aerosol dynamics [155], and sprays [156], to cite a few. In 2016, the original paper [121] in which the QMOM was developed was awarded the AS&T Outstanding Publication Award by the American Association for Aerosol Research.

C. DQMOM

The original QMOM can be only applied to problems with a univariate NDF due to the limitations of the Gaussian quadrature. One of the motivations for the DQMOM [127] was to develop an algorithm for solving the multivariate NDF transport equation. Another motivation was to achieve strong coupling between the abscissas and phase velocities, which will be discussed in section 3.2. The main difference of the DQMOM with other QBMMs is that it tracks directly the primary variables that appear in the quadrature approximation, rather than tracking the moments. In this section, we focus on the algorithm of the DQMOM for the univariate NDF transport equation, in which the difference between the DQMOM and the QMOM can be emphasized. It is straightforward to extend the DQMOM to problems with a multivariate NDF.

By substituting Eq. (23) into Eq. (2), the NDF transport equation can be written as follows:

$$\begin{aligned}&\sum_{i=0}^{N}\frac{\partial w_i\delta(d-d_i)}{\partial t}\\&\quad=\sum_{i=0}^{N}\delta(d-d_i)\frac{\partial w_i}{\partial t}-\sum_{i=0}^{N}w_i\delta'(d-d_i)\frac{\partial d_i}{\partial t}=S.\end{aligned} \tag{25}$$

Eq. (25) can be reformulated as

$$\begin{aligned}&\sum_{i=0}^{N}\delta(d-d_i)\frac{\partial w_i}{\partial t}\\&\quad-\sum_{i=0}^{N}\left(\delta'(d-d_i)\frac{\partial w_i d_i}{\partial t}-\delta'(d-d_i)d_i\frac{\partial w_i}{\partial t}\right)\\&\quad=\sum_{i=0}^{N}\left(\delta(d-d_i)+\delta'(d-d_i)d_i\frac{\partial w_i}{\partial t}\right)\\&\quad-\sum_{i=0}^{N}\left(\delta'(d-d_i)\frac{\partial w_i d_i}{\partial t}\right)=S.\end{aligned} \tag{26}$$

Applying the moment transform to Eq. (26) yields

$$\begin{aligned}&\int_0^{\infty}\left(\sum_{i=0}^{N}\left(\delta(d-d_i)+\delta'(d-d_i)d_i\frac{\partial w_i}{\partial t}\right)\right.\\&\left.\quad-\sum_{i=0}^{N}\left(\delta'(d-d_i)\frac{\partial w_i d_i}{\partial t}\right)\right)d^k\mathrm{d}d=S_k.\end{aligned} \tag{27}$$

Given that $\int d^k\delta(d-d_i)\mathrm{d}d=d_i^k$ and $\int d^k\delta'(d-d_i)\mathrm{d}d=-kd_i^{k-1}$, Eq. (27) can be simplified to the following:

$$(1-k)\sum_{i=0}^{N}d_i^k\frac{\partial w_i}{\partial t}+k\sum_{i=0}^{N}d_i^{k-1}\frac{\partial w_i d_i}{\partial t}=S_k, \tag{28}$$

which can be written in expanded form (e.g., $k=4$ and $N=$

2):

$$\begin{aligned}
\frac{\partial w_1}{\partial t} + \frac{\partial w_2}{\partial t} &= S_0, \\
\frac{\partial w_1 d_1}{\partial t} + \frac{\partial w_2 d_2}{\partial t} &= S_1, \\
-d_1^2\left(\frac{\partial w_1}{\partial t} + \frac{\partial w_2}{\partial t}\right) + 2d_2\left(\frac{\partial w_1 d_1}{\partial t} + \frac{\partial w_2 d_2}{\partial t}\right) &= S_2, \\
-2d_1^3\left(\frac{\partial w_1}{\partial t} + \frac{\partial w_2}{\partial t}\right) + 3d_2^2\left(\frac{\partial w_1 d_1}{\partial t} + \frac{\partial w_2 d_2}{\partial t}\right) &= S_3.
\end{aligned} \tag{29}$$

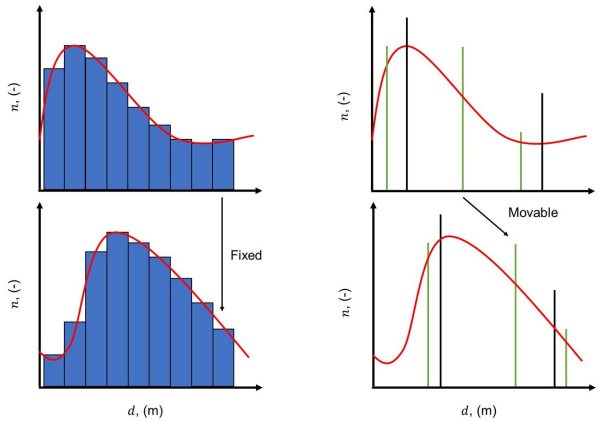

Fig. 2: Approximations of the real NDF (red solid lines) with two shapes (top and bottom) by the fixed-pivot CM (left) and the QMOM (right) with two abscissas (black solid lines) and three abscissas (green solid lines). The real NDF evolves with respect to time and its shape changes. In the QMOM, not only do the weights evolve with time but also the abscissas are free to move in the phase space. In the fixed-pivot CM, the particle size interval is defined in advance and particle sizes are fixed; only the weights of the particles evolve with respect to time.

Eq. (29) can be written in matrix form:

$$\begin{bmatrix} 1 & 1 & 0 & 0 \\ 0 & 0 & 1 & 1 \\ -d_1^2 & -d_1^2 & 2d_2 & 2d_2 \\ -2d_1^3 & -2d_1^3 & 3d_2^2 & 3d_2^2 \end{bmatrix} \begin{bmatrix} \frac{\partial w_1}{\partial t} \\ \frac{\partial w_2}{\partial t} \\ \frac{\partial w_1 d_1}{\partial t} \\ \frac{\partial w_2 d_2}{\partial t} \end{bmatrix} = \begin{bmatrix} S_0 \\ S_1 \\ S_2 \\ S_3 \end{bmatrix}. \tag{30}$$

Once the weights and the abscissas have been computed from the given initial moments, the source terms in Eq. (30) can be calculated in the same way as in the QMOM (see Eq. (22)). The matrix that is defined in the L.H.S. of Eq. (30), which is denoted as $\mathbf{A}$, depends only on the abscissas. If the abscissas are unique, $\mathbf{A}$ will be of full rank for arbitrary N. Subsequently, the unknown time derivative can be simply calculated by $\mathbf{A}^{-1}\mathbf{S}$:

$$\begin{bmatrix} \frac{\partial w_1}{\partial t} \\ \frac{\partial w_2}{\partial t} \\ \frac{\partial w_1 d_1}{\partial t} \\ \frac{\partial w_2 d_2}{\partial t} \end{bmatrix} = \begin{bmatrix} 1 & 1 & 0 & 0 \\ 0 & 0 & 1 & 1 \\ -d_1^2 & -d_1^2 & 2d_2 & 2d_2 \\ -2d_1^3 & -2d_1^3 & 3d_2^2 & 3d_2^2 \end{bmatrix}^{-1} \begin{bmatrix} S_0 \\ S_1 \\ S_2 \\ S_3 \end{bmatrix} = \begin{bmatrix} a_0 \\ a_1 \\ b_0 \\ b_1 \end{bmatrix}. \tag{31}$$

The solution procedure of the DQMOM is summarized as follows:

1) From the given initial moments, calculate the weights and abscissas by the moment inversion algorithm (e.g., the PD algorithm).
2) Calculate the source terms by Eq. (22) and construct the matrix $\mathbf{A}$ by Eq. (30).
3) Calculate the weights and abscissas by Eq. (31).
4) The iterative procedure is repeated from step 2.

The essence of the DQMOM is that the weights and abscissas are calculated and transported directly. Therefore, the moment inversion algorithm is only necessary for determining the weights and abscissas in step 1. This may be an advantage over the QMOM because the convergence problem in the moment inversion algorithm may be prevented. However, the successful computation of DQMOM is based on the assumption that the matrix $\mathbf{A}$ is full rank. When the abscissas are non-distinct, $\mathbf{A}$ is not full rank; it is singular. In such cases, Eq. (30) does not have a unique solution. In the context of QBMM, this means that not all the delta functions are needed to represent the NDF [127]. To overcome this problem, which is due to the identical node's values, it often suffices to add small perturbations to the non-distinct abscissas, so that $\mathbf{A}$ becomes full rank [127]. Due to its easy extension to problems with multivariate NDF, the DQMOM has been employed in many different applications [157]–[164].

D. EQMOM

The QMOM and the DQMOM employ the delta function to approximate the real NDF. In such cases, the continuous NDF is represented discontinuously. From a mathematical point of view, the real NDF is just a non-negative probability density function. Instead of using the Dirac delta function to approximate the NDF, the EQMOM approximates the NDF by a non-negative distribution function, such as the Gamma distribution function [129], Beta distribution function [129], Gaussian distribution function [148] or log-normal distribution function [165]. The distribution function is called the kernel density function (KDF) in the context of the EQMOM. Due to the capability of reconstructing a continuous NDF, the EQMOM has been applied extensively in problems in which the reconstruction of a continuous NDF is necessary [166]–[172]. In the following, the EQMOM with a log-normal KDF is presented as an example to investigate the algorithm. It is straightforward to employ other existing distribution functions as the KDF.

In the log-normal EQMOM, the NDF is approximated by

$$n(d) \approx \sum_{i=0}^{N} w_i \delta_\sigma(d, d_i), \tag{32}$$

where $\delta_\sigma(d, d_i)$ is the log-normal distribution function, which is expressed as follows:

$$\delta_\sigma(d, d_i) = \frac{1}{d\sigma\sqrt{2\pi}} \exp\left(-\frac{(\ln d - d_i)^2}{2\sigma^2}\right), \tag{33}$$

where σ is the variance of the log-normal distribution function; d_i and w_i are the abscissas and weights, which are usually called the primary abscissas and primary weights in the context of the EQMOM. The parameter σ is assumed to be the same for all the KDFs to obtain a single non-linear equation. The concept of the reconstructed continuous NDF of the EQMOM is presented in Fig.3. It can be seen that the continuous NDF that is reconstructed from the EQMOM overlaps the real NDF if the original real NDF follows a log-normal distribution function, whereas the QMOM only predicts three discontinuous abscissas.

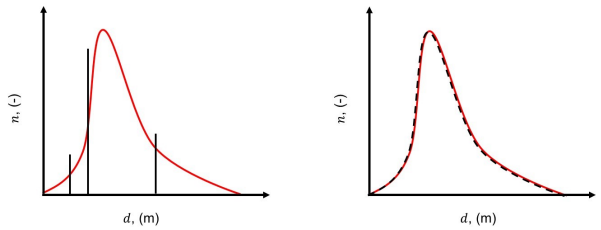

Fig. 3: Approximations for the real log-normal NDF (red solid line) by three nodes QMOM (left) and one primary node log-normal EQMOM (right). Black solid line: the abscissas of the QMOM. Black dashed line: reconstructed continuous NDF by the log-normal EQMOM.

The moment transport equations in the EQMOM can be derived in the same way as in the MOM or QMOM so they are identical to the equations that are reported in Eq. (5). Moreover, the source terms that are calculated by the EQMOM should be identical to them as well. One may, therefore, expect the mean particle size that are predicted by the EQMOM and the QMOM to be identical. However, because another unknown parameter σ in the EQMOM needs to be calculated, an additional moment equation is necessary to close the equation system. For simplicity, but without loss of generality, the algorithm of the log-normal EQMOM with two primary abscissas is discussed in the following section.

The moments of the NDF can be expressed by the analytical solution of the integral of the log-normal distribution function:

$$\begin{aligned} m_k &= \int_0^\infty \frac{w_1}{d\sigma\sqrt{2\pi}} \exp\left(-\frac{(\ln d - d_1)^2}{2\sigma^2}\right) \mathrm{d}d \\ &\quad + \int_0^\infty \frac{w_2}{d\sigma\sqrt{2\pi}} \exp\left(-\frac{(\ln d - d_2)^2}{2\sigma^2}\right) \mathrm{d}d \\ &= w_1 \exp\left(kd_1 + \frac{k^2\sigma^2}{2}\right) + w_2 \exp\left(kd_2 + \frac{k^2\sigma^2}{2}\right), \end{aligned} \quad (34)$$

which can be written in the following expanded form (e.g., $N = 5$):

$$\begin{aligned} m_0 &= w_1 + w_2 \\ m_1 &= w_1 e^{\left(d_1 + \frac{\sigma^2}{2}\right)} + w_2 e^{\left(d_2 + \frac{\sigma^2}{2}\right)} \\ m_2 &= w_1 e^{\left(2d_1 + 2\sigma^2\right)} + w_2 e^{\left(2d_2 + 2\sigma^2\right)} \\ m_3 &= w_1 e^{\left(3d_1 + \frac{9\sigma^2}{2}\right)} + w_2 e^{\left(3d_2 + \frac{9\sigma^2}{2}\right)} \\ m_4 &= w_1 e^{\left(4d_1 + \frac{16\sigma^2}{2}\right)} + w_2 e^{\left(4d_2 + \frac{16\sigma^2}{2}\right)} \end{aligned} \quad (35)$$

Eq. (35) is closed for five unknown parameters with five equations. Directly solving Eq. (35) requires a non-linear solver, which is computational-resource demanding. However, if we eliminate w_1, w_2, d_1, and d_2 from Eq. (35), a polynomial equation of σ can be found. Unfortunately, it is not convenient to obtain the analytical solution of the polynomial equation due to the highly non-linear dependence on σ. An iterative root finding procedure, such as Ridder's method [129], [151], can be employed to update σ. Setting

$$z = e^{\frac{\sigma^2}{2}}, \xi_1 = e^{d_1}, \xi_2 = e^{d_2}, \quad (36)$$

Eq. (35) leads to

$$\begin{aligned} m_0 &= w_1 + w_2 = m_0^*, \\ m_1 &= z\left(w_1\xi_1 + w_2\xi_2\right) = z m_1^*, \\ m_2 &= z^4\left(w_1\xi_1^2 + w_2\xi_2^2\right) = z^4 m_2^*, \\ m_3 &= z^9\left(w_1\xi_1^3 + w_2\xi_2^3\right) = z^9 m_3^*, \\ m_4 &= z^{16}\left(w_1\xi_1^4 + w_2\xi_2^4\right) = z^{16} m_4^*. \end{aligned} \quad (37)$$

where m_k^* is mathematically equivalent to the moments that are defined in the QMOM in which the NDF is approximated by a delta function. The σ finding procedure consists of the following main steps: Calculate the corresponding m_k and m_k^* from a given initial σ. Update the primary weights and abscissas from the first four m_k^* by the moment inversion algorithm. Determine whether the given initial value of σ satisfies the fifth equation in Eq. (37), namely

$$f(\sigma) = m_4 - e^{8\sigma^2} m_4^* \stackrel{?}{=} 0, \quad (38)$$

where m_4 is the given initial moment and m_4^* equals $\sum_{i=1}^5 w_i\xi_1$. If $f(\sigma)$ is smaller than the machine tolerance, the guessed value of σ satisfies Eq. (37). Ridder's method can be used to find the root of Eq. (38), which is σ. The details of Ridder's method can be found in the literature [151]. Here, we only summarise the iterative procedure that was applied to the EQMOM:

1) Calculate the midpoint $\sigma_3 = 0.5(\sigma_1 + \sigma_2)$ from two given initial roots, σ_1 and σ_2.
2) Calculate σ_4 by

$$\sigma_4 = \sigma_3 + (\sigma_3 - \sigma_1)\frac{\mathrm{sign}\left(f(\sigma_1) - f(\sigma_2)\right) f(\sigma_3)}{\sqrt{f(\sigma_3)^2 - f(\sigma_1)f(\sigma_2)}}. \quad (39)$$

3) Check whether $f(\sigma_4) = 0$. If yes, the iterative procedure converges. Otherwise, repeat the iterative procedure from step 1.

After σ has been found, the continuous NDF can be constructed by Eq. (32). To calculate the moments for the next time step, the source terms need to be calculated. One may want to calculate the source terms in the EMOM following the procedure that was employed in the QMOM. However, even the moment transport equations for the EQMOM are identical with the equations in the QMOM, the closure in the EQMOM is much more complicated than in the QMOM due to the continuous reconstructed NDF. In the following, the breakage source terms were employed as an example to demonstrate that secondary abscissas and weights need to be introduced to calculate the source terms.

The death term of the breakage can be calculated by

$$\begin{aligned}\int_0^\infty d^k g\left(d\right) n\left(d\right) \mathrm{d}d &= \int_0^\infty d^k g\left(d\right) \left(\sum_{i=0}^{N} w_i \delta_\sigma(d,d_i)\right) \mathrm{d}d \\ &= \sum_{i=1}^{N} w_i \int_0^\infty d^k g\left(d\right) \delta_\sigma(d,d_i) \mathrm{d}d \\ = \sum_{i=1}^{N} w_i \int_0^\infty d^k g\left(d\right) \frac{1}{d\sigma\sqrt{2\pi}} \exp\left(-\frac{\left(\ln d - d_i\right)^2}{2\sigma^2}\right) \mathrm{d}d.\end{aligned} \tag{40}$$

Define

$$\begin{aligned}s^2 = \frac{\left(\ln d - d_i\right)^2}{2\sigma^2} &\rightarrow d = \exp(\sigma s\sqrt{2} + d_i) \\ &\rightarrow \mathrm{d}d = \sqrt{2}\sigma \exp(\sigma s\sqrt{2} + d_i)\mathrm{d}s.\end{aligned} \tag{41}$$

Substitute Eq. (41) into Eq. (40):

$$\begin{aligned}&\sum_{i=1}^{N} w_i \int_0^\infty d^k g\left(d\right) \frac{1}{d\sigma\sqrt{2\pi}} \exp\left(-\frac{\left(\ln d - d_i\right)^2}{2\sigma^2}\right) \mathrm{d}d \\ &= \sum_{i=1}^{N} w_i \int_{-\infty}^{\infty} \frac{\left(\exp(\sigma s\sqrt{2} + d_i)\right)^k g\left(\exp(\sigma s\sqrt{2} + d_i)\right)}{\exp(\sigma s\sqrt{2} + d_i)\sigma\sqrt{2\pi}} \\ &\qquad e^{-s^2}\sqrt{2}\exp(\sigma s\sqrt{2} + d_i)\mathrm{d}s \\ &= \frac{1}{\sqrt{\pi}} \sum_{i=1}^{N} w_i \int_{-\infty}^{\infty} \left(\exp(\sigma s\sqrt{2} + d_i)\right)^k \\ &\qquad g\left(\exp(\sigma s\sqrt{2} + d_i)\right) e^{-s^2}\mathrm{d}s.\end{aligned} \tag{42}$$

Eq. (42) can be calculated by the Gauss-Hermite formula:

$$\begin{aligned}&\frac{1}{\sqrt{\pi}} \sum_{i=1}^{N} w_i \int_{-\infty}^{\infty} \left(\exp(\sigma s\sqrt{2} + d_i)\right)^k \\ &\qquad g\left(\exp(\sigma s\sqrt{2} + d_i)\right) e^{-s^2}\mathrm{d}s \\ &= \frac{1}{\sqrt{\pi}} \sum_{i=1}^{N} w_i \left(\sum_{j=1}^{N_j} \left(\exp(\sigma s_j\sqrt{2} + d_i)\right)^k \right. \\ &\qquad \left. g\left(\exp(\sigma s_j\sqrt{2} + d_i)\right) w_j\right),\end{aligned} \tag{43}$$

TABLE II: The numbers of the summation operations for the QMOM and the EQMOM with different numbers of abscissas.

	Number of nodes and weights	Number of summation operation
QMOM	$N = 2$	4
	$N = 3$	9
EQMOM	$N = 2$, $N' = 10$	400
	$N = 2$, $N' = 20$	1600

where N_j is the number of the secondary abscissas s_j and weights w_j. Eq. (43) is the final form of the death term of the breakage in the EQMOM. It can be seen that s_j and w_j are introduced in order to calculated the integral in Eq. (43). We can choose a large value of N_j to improve the accuracy of Eq. (43). The calculation of other terms is neglected here for brevity. The final breakage and coalescence source terms are reported as follows:

$$\begin{aligned}\overline{S}_k \approx &\frac{1}{2\pi} \sum_{i_1=1}^{N} \sum_{i_2=1}^{N} w_{i_1} w_{i_2} \sum_{j_1=1}^{N_j} \sum_{j_2=1}^{N_j} w_{j_1} w_{j_2} \\ &\left[\left(\epsilon_{i_1,j_1}^3 + \epsilon_{i_2,j_2}^3\right)^{k/3} - \epsilon_{i_1,j_1}^k - \epsilon_{i_2,j_2}^k\right] a_{i_1,j_1,i_2,j_2} \\ &+ \frac{1}{\sqrt{\pi}} \sum_{i_1=1}^{N} \sum_{j_1=1}^{N^*} w_{i_1} w_{j_1}^* g_{i_1,j_1} \left(\overline{b}_{i_1,j_1}^k - \epsilon_{i_1,j_1}^k\right),\end{aligned} \tag{44}$$

where $a_{i_1,j_1,i_2,j_2} = a(\epsilon_{i_1,j_1}, \epsilon_{i_2,j_2})$, $g_{i_1,j_1} = g(\epsilon_{i_1,j_1})$, and where:

$$\overline{b}_{i_1,j_1}^k = \int_0^\infty d^k \beta\left(d|\epsilon_{i_1,j_1}\right) \mathrm{d}d, \epsilon_{i_1,j_1} = \epsilon(s_j, d_i) \tag{45}$$

The solution procedure of the EQMOM is summarized as follows:

1) Guess σ, calculate the corresponding m_k^* by Eq. (37) from the given first even initial moments. Calculate the primary weights and abscissas by the moment inversion algorithm (e.g., the PD algorithm).
2) Determine whether the convergence criterion is satisfied, which is given in Eq. (38). If yes, calculate the source terms. Otherwise, apply Ridder's iterative procedure until the convergence criterion is satisfied.
3) Calculate the source terms and the unknown time derivatives of the moments in Eq. (22).
4) The iterative procedure is repeated from step 1.

In contrast to the QMOM, the EQMOM employs $2N + 1$ moments to calculate the N primary weights and abscissas, and an additional parameter σ, which can be used to reconstruct a continuous NDF. Obviously, the additional moment transport equation imposes increased computational resource requirement. In addition, an iterative procedure with the Ridder's method is carried out in each time-step loop. This dual-iterative feature of the EQMOM leads to slow calculation. Sometimes the calculations diverge, depending on the initial guess for σ. However, it was found that most of the computational resources were spent on the calculation of the

source terms [24] and the EQMOM can be much slower than other QBMMs, such as the DQMOM or even the CM [173]. As reported in Table. II, there are only $N \times N$ summation operations for the coalescence source terms for the QMOM. However, for the EQMOM with N primary abscissas and N' secondary abscissas, there are $(N \times N') \times (N \times N')$ summation operations for the coalescence source terms.

E. CQMOM

The CQMOM was first introduced and validated for passive scalars transportation [120] for Flash Nanoprecipitation. One year later, the comprehensive theory of the CQMOM was presented by Yuan et al. [128], and it was applied to active scalars (e.g., velocities). Compared with the QMOM and the EQMOM and other methods (e.g., the multivariate QMOM [140], the tensor-product QMOM [141] or the DQMOM), the CQMOM is a more popular method for problems with multivariate NDF. It is based on conditional density function (CDF) theory. The CDF represents the probability of having one internal coordinate within an infinitesimal limit when one or more of the other internal coordinates are fixed and equal to a specific value [73], [128]. For clarity, we will only discuss the algorithm of the CQMOM with two internal coordinates, namely, particle size d and particle composition ϕ. Moreover, two abscissas for the particle size and composition are employed as an example to demonstrate the algorithm of the CQMOM. It is straightforward to increase the number of internal coordinates for other problems.

The bivariate NDF, which is denoted as $n(d, \phi)$, can be written as

$$n(d, \phi) = n(\phi|d)n(d), \tag{46}$$

where $n(\phi|d)$ corresponds to the CDF for ϕ given a fixed value of d. Therefore, the conditional moments for ϕ are defined by

$$\langle \phi \rangle^j (d_\alpha) = \int \phi^j n(\phi|d_\alpha) \mathrm{d}\phi = \sum_{\beta=1}^{N_\beta} w_{\alpha,\beta} \phi_{\alpha,\beta}^j, \tag{47}$$

where $w_{\alpha,\beta}$ and $\phi_{\alpha,\beta}$ are the conditional weights and abscissas for ϕ, respectively; N_β is the number of the abscissas for ϕ. Eq. (47) implies that any given value of d_α corresponds to a conditional moment set $\langle \phi \rangle^j (d_\alpha)$. The conditional moment set can be used to find the conditional weights and abscissas for the conditioned internal coordinate. It is straightforward to show that

$$\begin{aligned} m_{i,j} &= \int\int d^i \phi^j n(d, \phi) \mathrm{d}d\mathrm{d}\phi \\ &= \int d^i \left(\int \phi^j n(\phi|d) \mathrm{d}\phi \right) n(d) \mathrm{d}d \\ &= \sum_{\alpha=1}^{N_\alpha} w_\alpha d_\alpha^i \left(\int \phi^j n(\phi|d_\alpha) \mathrm{d}\phi \right) = \sum_{\alpha=1}^{N_\alpha} w_\alpha d_\alpha^i \langle \phi \rangle^j (d_\alpha) \\ &= \sum_{\alpha=1}^{N_\alpha} w_\alpha d_\alpha^i \left(\sum_{\beta=1}^{N_\beta} w_{\alpha,\beta} \phi_{\alpha,\beta}^j \right), \end{aligned} \tag{48}$$

where N_α is the number of abscissas for d. Eq. (48) can be used to find the conditional weights and abscissas for the conditional (secondary) internal coordinate from the pure moments ($m_{i,0}$). For example, if $j = 0$, the weights and abscissas can be calculated by the moment inversion algorithm as discussed in the previous sections:

$$\begin{bmatrix} m_{0,0} \\ m_{1,0} \\ m_{2,0} \\ m_{3,0} \end{bmatrix} \overset{\text{PD}}{\rightarrow} \begin{bmatrix} w_1 \\ w_2 \\ d_1 \\ d_2 \end{bmatrix}. \tag{49}$$

After the weights and abscissas have been found, the conditional weights and abscissas for the second internal coordinate can be calculated from the conditional moments by Eq. (47). These unknown conditional moments can be calculated by Eq. (48). For example, after d_1 and d_2 have been calculated, the conditional moments $\langle \phi \rangle^j (d_\alpha)$ can be calculated by Eq. (48), which can be written as the following expanded form (e.g., $N_\alpha = N_\beta = 2$):

$$\begin{aligned} m_{0,1} &= w_1 \langle \phi \rangle^1 (d_1) + w_2 \langle \phi \rangle^1 (d_2), \\ m_{1,1} &= w_1 d_1 \langle \phi \rangle^1 (d_1) + w_2 d_2 \langle \phi \rangle^1 (d_2), \\ m_{0,2} &= w_1 \langle \phi \rangle^2 (d_1) + w_2 \langle \phi \rangle^2 (d_2), \\ m_{1,2} &= w_1 d_1 \langle \phi \rangle^2 (d_1) + w_2 d_2 \langle \phi \rangle^2 (d_2), \\ m_{0,3} &= w_1 \langle \phi \rangle^3 (d_1) + w_2 \langle \phi \rangle^3 (d_2), \\ m_{1,3} &= w_1 d_1 \langle \phi \rangle^3 (d_1) + w_2 d_2 \langle \phi \rangle^3 (d_2). \end{aligned} \tag{50}$$

Eq. (50) can be written in the following matrix form:

$$\begin{bmatrix} \langle \phi \rangle^j (d_1) \\ \langle \phi \rangle^j (d_2) \end{bmatrix} = \begin{bmatrix} w_1 & w_2 \\ w_1 d_1 & w_2 d_2 \end{bmatrix}^{-1} \begin{bmatrix} m_{0,j} \\ m_{1,j} \end{bmatrix} \tag{51}$$

As long as the abscissas d_i are distinct, the Vandermonde linear system in Eq. (51) is of full rank and the necessary conditional moments $\langle \phi \rangle^j (d_1)$ and $\langle \phi \rangle^j (d_2)$ can be calculated. By virtue of Eq. (47), the conditional weights and abscissas can be calculated by the following relationship:

$$\begin{bmatrix} \langle \phi \rangle^0 (d_1) \\ \langle \phi \rangle^1 (d_1) \\ \langle \phi \rangle^2 (d_1) \\ \langle \phi \rangle^3 (d_1) \end{bmatrix} \overset{\text{PD}}{\rightarrow} \begin{bmatrix} w_{1,1} \\ w_{1,2} \\ \phi_{1,1} \\ \phi_{1,2} \end{bmatrix}, \begin{bmatrix} \langle \phi \rangle^0 (d_2) \\ \langle \phi \rangle^1 (d_2) \\ \langle \phi \rangle^2 (d_2) \\ \langle \phi \rangle^3 (d_2) \end{bmatrix} \overset{\text{PD}}{\rightarrow} \begin{bmatrix} w_{2,1} \\ w_{2,2} \\ \phi_{2,1} \\ \phi_{2,2} \end{bmatrix}. \tag{52}$$

The calculation of the source terms in the CQMOM needs to take into account the multivariate NDF. For example, the source terms for the breakage and coalescence processes are

expressed as follows [6], [174]:

$$
\begin{aligned}
S(d,\phi) = \frac{d^2}{2}\int_0^d\int_0^\phi & \frac{a\left((d^3-d'^3)^{1/3},d'\right)}{(d^3-d'^3)^{2/3}} \\
& n\left((d^3-d'^3)^{1/3},(\phi-\phi_{d'})\right) n(d',\phi_{d'})\,\mathrm{d}d'\,\mathrm{d}\phi_{d'} \\
& - n(d,\phi)\int_0^\infty a(d,d')n(d',\phi_{d'})\,\mathrm{d}d'\,\mathrm{d}\phi_{d'} \\
& + \int_d^\infty\int_\phi^\infty g\left(d'\right)\beta\left(d,\phi|d',\phi_{d'}\right)n\left(d',\phi_{d'}\right)\,\mathrm{d}d'\,\mathrm{d}\phi_{d'} \\
& - g\left(d\right)n\left(d,\phi\right), \quad (53)
\end{aligned}
$$

Eq. (53) is different from Eq. (15) due to the existence of the multivariate NDF, and the closure is different. Moreover, the DSD function needs to be extended. Readers who are interested in the theory are referred to the latest works [6], [73] for comprehensive information. Here, we employ the death term and the birth term of the breakage source term as an example, to demonstrate the calculation procedure. The breakage sink term can be calculated as follows:

$$
\begin{aligned}
\int_0^\infty\int_0^\infty & d^i\phi^j g\left(d\right)n\left(d,\phi\right)\mathrm{d}d\mathrm{d}\phi \\
& = \int_0^\infty d^i g\left(d\right)\left(\int_0^\infty \phi^j n\left(\phi|d\right)\mathrm{d}\phi\right)n(d)\mathrm{d}d \\
& = \sum_{\alpha=1}^{N_\alpha} d_\alpha^i g(d_\alpha) w_\alpha \left(\sum_{\beta=1}^{N_\beta}\phi_{\alpha,\beta}^j w_{\alpha,\beta}\right). \quad (54)
\end{aligned}
$$

The breakage source term can be calculated as follows:

$$
\begin{aligned}
\int_0^\infty\int_0^\infty & d^i\phi^j \int_d^\infty\int_\phi^\infty g\left(d'\right)\beta\left(d,\phi|d',\phi_{d'}\right)n\left(d',\phi_{d'}\right)\,\mathrm{d}d'\,\mathrm{d}\phi_{d'}\,\mathrm{d}d\,\mathrm{d}\phi \\
& = \int_0^\infty n(d')g(d')\left(\int_0^\infty n(\phi_{d'}|d'))\left(\int_0^{d'}\int_0^{\phi_{d'}} d^i\phi^j\beta\left(d,\phi|d',\phi_{d'}\right)\mathrm{d}d\,\mathrm{d}\phi\right)\,\mathrm{d}\phi_{d'}\right)\,\mathrm{d}d' \\
& = \sum_{\alpha=1}^{N_\alpha} w_\alpha g(d_\alpha)\left(\sum_{\beta=1}^{N_\beta} w_{\alpha,\beta}\left(\int_0^{d_\alpha}\int_0^{\phi_{\alpha,\beta}} d^i\phi^j\beta\left(d,\phi|d_\alpha,\phi_{\alpha,\beta}\right)\mathrm{d}d\,\mathrm{d}\phi\right)\right). \quad (55)
\end{aligned}
$$

For a given bivariate DSD function [6]:

$$
\begin{aligned}
& \beta\left(d,\phi|d_\alpha,\phi_{\alpha,\beta}\right) \\
& \quad = 180\frac{d^2}{d_\alpha^3}\left(\frac{d^3}{d_\alpha^3}\right)^2\left(1-\frac{d^3}{d_\alpha^3}\right)^2\delta\left(\phi-\frac{d^3}{d_\alpha^3}\phi_{\alpha,\beta}\right), \quad (56)
\end{aligned}
$$

the analytical solution can be calculated by

$$
\begin{aligned}
\int_0^{d_\alpha}\int_0^{\phi_{\alpha,\beta}} & d^i\phi^j\beta\left(d,\phi|d_\alpha,\phi_{\alpha,\beta}\right)\mathrm{d}d\,\mathrm{d}\phi \\
& = 3240\frac{d_\alpha^i\phi_{\alpha,\beta}^j}{(i+3j+9)(i+3j+12)(i+3j+15)}. \quad (57)
\end{aligned}
$$

By grouping Eq. (57), Eq. (55) and Eq. (54), the breakage source terms can be written as

$$
\begin{aligned}
S_{i,j}^{br} = & \sum_{\alpha=1}^{N_\alpha} w_\alpha g(d_\alpha) \\
& \sum_{\beta=1}^{N_\beta}\frac{3240 w_{\alpha,\beta} d_\alpha^i\phi_{\alpha,\beta}^j}{(i+3j+9)(i+3j+12)(i+3j+15)} \\
& - \sum_{\alpha=1}^{N_\alpha} d_\alpha^i g(d_\alpha) w_\alpha \sum_{\beta=1}^{N_\beta}\phi_{\alpha,\beta}^j w_{\alpha,\beta}. \quad (58)
\end{aligned}
$$

As illustrated in Fig. 4, the solution procedure of the CQMOM is summarized as follows:

1) Calculate the abscissas and weights for the first internal coordinate from the given initial pure moments.
2) Construct the Vandermonde matrix from the abscissas and the weights.
3) From the Vandermonde matrix and the given initial mixed moments on the second internal coordinate, calculate the conditional moments $\langle\phi\rangle^j\left(d_\alpha\right)$ by Eq. (51).
4) From the calculated conditional moments, calculate the conditional abscissas and the weights by the moment inversion algorithm. Calculate the source terms by Eq. (58).

5) The iterative procedure is repeated from step 1.

As an algorithm for problems with a multivariate NDF, the CQMOM is suitable and applicable for simulating the multiphase system with mass transfer [174], [175] and chemical reactions [176], in which the internal coordinates include particle size and composition. In addition, the CQMOM is extensively applied to the multi-dimensional KE for gas-particle flows, in which the velocity components (e.g., u and v) can be treated as different internal coordinates. For such flows, the most obvious manifestation of non-equilibrium behavior is particle trajectory crossing (PTC), which can be only predicted with multiple velocity nodes by the CQMOM. In such cases, particles with the same size can be transported with different velocities (abscissas). Readers who are interested in this subject are referred to other works [128], [148], [171], [177].

F. ECQMOM

The CQMOM can be considered as an improved QMOM-based method for problems with a multivariate NDF. In such cases, the NDF is discontinuously approximated. Is it possible to merge the CQMOM with the EQMOM to predict the continuous multivariate NDF? The answer to this question seems to be yes. The ECQMOM concept was first developed and applied for gas-particle flows in the 2D large eddy simulation (LES) framework by [148] and was discussed in detail by [73]. In the work of Chalons et al. [148], the ECQMOM with Gaussian KDF was called multi-Gaussian (MG) quadrature method. Because they aimed at LES, only the ECQMOM can capture the velocity dispersion around each quadrature point [166], [171], [178]. Similar to the EQMOM, the multivariate NDF in the ECQMOM is approximated by

$$n(d,\phi) \approx \sum_{\alpha=1}^{N_\alpha} w_\alpha \delta_\sigma\left(d, d_\alpha\right)\left(\sum_{\beta=1}^{N_\beta} w_{\alpha,\beta}\delta_{\sigma_\alpha}\left(\phi,\phi_{\alpha,\beta}\right)\right), \tag{59}$$

where σ and σ_α are the variances for the first internal coordinate and the second internal coordinate, respectively. To solve for these two additional unknown variances in the unclosed equation system, two additional moment equations are necessary. The solution procedure of the ECQMOM is illustrated in Fig. 4. The calculations of the source terms and the moment transport equations are similar to the CQMOM and the EQMOM. Therefore, the calculation procedure of the ECQMOM is omitted here for simplicity.

III. CFD-PBE COUPLING FOR INHOMOGENEOUS MULTIPHASE SYSTEMS

All the algorithms that were discussed above can be extended for spatially inhomogeneous multiphase systems. In such cases, the flow field information (e.g., turbulent energy dissipation rate) needs to be specified. The information of the flow field is usually provided by the CFD simulation. Then, a CFD-PBE coupling procedure should be formulated. The CFD-PBE coupling can be implemented in any CFD code, such as ANSYS Fluent or OpenFOAM. Recently, an open-source OpenFOAM-based code which is called OpenQBMM was released. The QMOM, EQMOM and CQMOM were implemented with multiple sub-models [179]. In the coupled CFD-PBE system, a corresponding spatial advection term and a diffusion term for fine particles [73], [180] need to be included, which will be discussed in the following sections.

A. CFD coupling with the QMOM and the EQMOM

In the QMOM and EQMOM in which the moments are transported, the moment advection terms and diffusion terms (for fine particles) should be included. Take the advection term as an example. If we apply the moment transformation in Eq. (3), the moment transport equations can be written as follows:

$$\frac{\partial m_k}{\partial t} + \nabla\cdot\left(\mathbf{U}_\mathrm{d} m_k\right) = S_k, \tag{60}$$

where S_k is the integral form of the source term, $\mathbf{U}_\mathrm{d}$ is the dispersed phase velocity, which can be predicted by the CFD. Depending on the specific problem, Eq. (60) needs to be addressed separately. If it is coupled with a single-phase CFD solver, it is common to implement the moment transport equations as passive scalar transport equations, which can be viewed as a type of one-way coupling. In such cases, the solution of the PBE has no effect on the flow field and the implementation is straightforward. If it is coupled with a two-phase CFD solver, in which the PBE is used to describe the dispersed phase's movement and evolution, $\mathbf{U}_\mathrm{d}$ can be calculated by the two-phase CFD solver (e.g., two-fluid model) and the effect of the particle size on the interfacial force exchange term needs to be considered. In the incompressible two-fluid model (TFM) without mass and heat transfer, the governing equations are reported by [181]–[183]

$$\frac{\partial \alpha_\mathrm{d}}{\partial t} + \nabla\cdot\left(\alpha_\mathrm{d}\mathbf{U}_\mathrm{d}\right) = 0, \tag{61}$$

$$\frac{\partial\left(\alpha_\mathrm{d}\mathbf{U}_\mathrm{d}\right)}{\partial t} + \nabla\cdot\left(\alpha_\mathrm{d}\left(\mathbf{U}_\mathrm{d}\otimes\mathbf{U}_\mathrm{d}\right)\right) + \nabla\cdot\left(\alpha_\mathrm{d}\tau_\mathrm{d}\right) + \nabla\cdot\left(\alpha_\mathrm{d}\mathbf{R}_\mathrm{d}\right) = -\alpha_\mathrm{d}\nabla p + \alpha_\mathrm{d}\mathbf{g} + \mathbf{M}_\mathrm{d}, \tag{62}$$

$$\frac{\partial\left(\alpha_\mathrm{c}\mathbf{U}_\mathrm{c}\right)}{\partial t} + \nabla\cdot\left(\alpha_\mathrm{c}\left(\mathbf{U}_\mathrm{c}\otimes\mathbf{U}_\mathrm{c}\right)\right) + \nabla\cdot\left(\alpha_\mathrm{c}\tau_\mathrm{c}\right) + \nabla\cdot\left(\alpha_\mathrm{c}\mathbf{R}_\mathrm{c}\right) = -\alpha_\mathrm{c}\nabla p + \alpha_\mathrm{c}\mathbf{g} - \mathbf{M}_\mathrm{d}, \tag{63}$$

where α_d is the volume fraction of the dispersed phase, ρ_d is its density and $\mathbf{U}_\mathrm{d}$ is its average velocity, p is the pressure shared by the two phases, τ_d and τ_c are the viscous-stress tensors, $\mathbf{R}_\mathrm{d}$ and $\mathbf{R}_\mathrm{c}$ are the Reynolds-stress tensors, $\mathbf{g}$ is the gravitational acceleration vector and $\mathbf{M}_\mathrm{d}$ is the interfacial force term. The CFD-PBE coupling lies in the calculation of the $\mathbf{M}_\mathrm{d}$. In the TFM, the particle size is assumed to be constant. However, in the CFD-PBE coupling, the mean Sauter diameter for each computational grid is calculated from the predicted abscissas and weights, and the growth and breakage/coalescence can be included. Moreover, it is common for strong breakage and coalescence to occur in the turbulent mixing processes. The TFM will fail in predicting such a phenomenon.

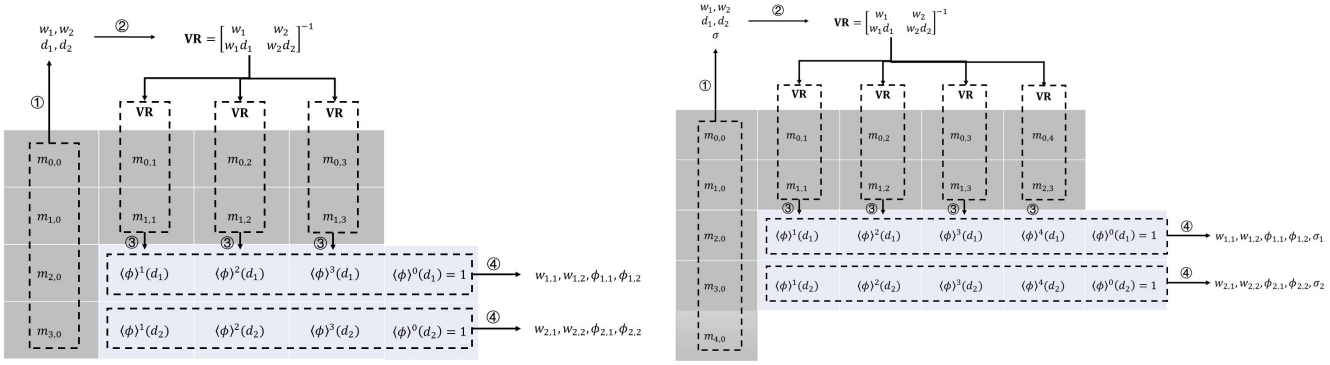

Fig. 4: Solution procedure for CQMOM (left) and ECQMOM (right) with two internal coordinates (d and ϕ). The elements in gray were given as the initial mixed moments ($m_{i,j}$).

The coupling of CFD with the moment transport equations is summarized as follows:

1) Calculate the interfacial force exchange term (e.g., drag force) from the mean Sauter diameter, which is computed from the initial moments (e.g., m_3/m_2).
2) Calculate the information of the flow field by the TFM with the updated interfacial force exchange term.
3) Feed the calculated advection velocity into the moment transport equations and update the moments for the next time step.
4) The iterative procedure is repeated from step 1.

The coupling of CFD with the moment transport equations is suitable for a large variety of applications. However, it can be seen that all moments are transported with the same dispersed velocity, as reported in Eq. (60). Thus, all particles are moving with the same velocity: $\mathbf{U}_\mathrm{d}$. This approximation is only applicable when the Stokes number is sufficiently small that the shape of the NDF is generally narrow enough not to have a significant size-segregation effect.

B. CFD coupling with the DQMOM

If the DQMOM is employed to solve the PBE, another coupling procedure is required because the moment transport equations are transformed to the weights/abscissas transport equations. The weights and abscissas can be transported with different velocities, which is another important feature of the DQMOM. The coupling is therefore applicable for the problems with a wide NDF shape. Extending the homogeneous DQMOM algorithm to the inhomogeneous DQMOM is straightforward; only the advection term needs to be included in Eq. (31), which can be written as follows:

$$\begin{bmatrix} \frac{\partial w_1}{\partial t} + \nabla \cdot (w_1 \mathbf{U}_1) \\ \frac{\partial w_2}{\partial t} + \nabla \cdot (w_2 \mathbf{U}_2) \\ \frac{\partial w_1 d_1}{\partial t} + \nabla \cdot (w_1 d_1 \mathbf{U}_1) \\ \frac{\partial w_2 d_2}{\partial t} + \nabla \cdot (w_2 d_2 \mathbf{U}_2) \end{bmatrix} = \begin{bmatrix} a_0 \\ a_1 \\ b_0 \\ b_1 \end{bmatrix} \tag{64}$$

where $\mathbf{U}_1$ and $\mathbf{U}_2$ are the advection velocities for the first abscissa and second abscissa, respectively. If we assume

$$\mathbf{U}_1 = \mathbf{U}_2 = \mathbf{U}_\mathrm{d}, \tag{65}$$

the predicted abscissas and weights by the DQMOM will be identical to the results that are predicted by the moment transport equations as reported in Eq. (60). However, Eq. (65) goes against the motivation of developing the DQMOM to strongly couple the internal coordinates with the phase velocities. To predict the different phase velocities for different internal coordinates, the DQMOM is usually coupled with the multi-fluid model (MFM) instead of the TFM, where only one dispersed phase velocity is predicted.

C. CFD coupling with the CQMOM and ECQMOM

In the moment transport equations in the CQMOM and the ECQMOM, special treatments need to be included, depending on the specific problems. If the phase-space diffusion is neglected, it is enough to add the advection terms into the mixed moment transport equations as reported in Fig. 4. If $N_1 = 2$ and $N_2 = 2$, ten and thirteen moment transport equations need to be solved for the CQMOM and the ECQMOM, respectively. This coupling procedure is similar to the coupling of CFD with QMOM/EQMOM. The CQMOM and ECQMOM was applied to simulate Flash Nanoprecipitation and droplet evaporation [120], [156]. However, for the mass transfer of species when chemical reactions occur, the phase-space diffusion terms should be included [174], [175]. For such problems, the drift terms should be added into the NDF transport equation reported in Eq. (1):

$$\frac{\partial n(d,\phi)}{\partial t} + \nabla \cdot (\mathbf{U}_\mathrm{d} n(d,\phi)) + \nabla_\phi \left(\dot{\phi} n(d,\phi) \right) = S \tag{66}$$

where $\dot{\phi}$ is the rate of continuous change of particle composition due to molecular phenomena. Transforming the third term in the L.H.S. of Eq. (66) to the moment terms follows the same procedure as that reported in Eq. (7). Another important application of the CQMOM is to solve the transport equation of the velocity distribution function (VDF) to capture the PTC, which can be only predicted by multiple values of the advection velocities. However, it should be stressed here that the PBE is not suitable for such processes, and the coupling procedure that was discussed here is not suitable for predicting PTC because the velocity is excluded from the

internal coordinate. As the discussion of the CFD coupling with the KE is beyond of the scope of this work, readers who are interested in this subject are referred to other works [128].

IV. Numerical problems and limitations

A. Boundedness of the phase fraction and moments

The moments of the NDF represent some important physical properties of the population of particles and they have to obey physical rules. For example, when the internal coordinate is the particle diameter, m_3 is linearly dependent on the phase fraction:

$$m_3 = k_v \alpha, \tag{67}$$

where k_v is the shape coefficient which equals $\pi/6$ for a sphere particle. Under such assumption, the transport equation of m_3 (without source terms) is equivalent to the dispersed phase fraction transport equation, which implies

$$\frac{\partial m_3}{\partial t} + \nabla \cdot (\mathbf{U}_\mathrm{d} m_3) = 0 \tag{68}$$

equals

$$\frac{\partial \alpha_\mathrm{d}}{\partial t} + \nabla \cdot (\mathbf{U}_\mathrm{d} \alpha_\mathrm{d}) = 0. \tag{69}$$

When Eq. (68) and Eq. (69) are solved by the finite volume method, the key issue is to ensure the boundedness of m_3 and the phase fraction, as unbounded solutions may look reasonable but are completely erroneous. By close examination of Eq. (69), the use of the upwind approximation can guarantee that the phase fraction is bounded by zero, but it cannot guarantee that it is bounded by one. If the phase equations for both phases are solved together and an appropriate bounded discretization scheme is applied, $\alpha \geqslant 0$ and the constraint $\alpha \leqslant 1$ will be obeyed [184]. However, this method does not guarantee conservation, which is a critical issue in multiphase flows with high density ratios because small phase fraction errors may correspond to large mass-fraction errors. Weller [185] proposed using the following equation instead of the original one:

$$\frac{\partial \alpha_\mathrm{d}}{\partial t} + \nabla \cdot (\mathbf{U} \alpha_\mathrm{d}) - \nabla \cdot (\mathbf{U}_\mathrm{r} (1 - \alpha_\mathrm{d}) \alpha_\mathrm{d}) = 0, \tag{70}$$

where $\mathbf{U}_\mathrm{r}$ is the relative phase velocity and $\mathbf{U}$ is the average phase velocity, which equals $\alpha_\mathrm{d}\mathbf{U}_\mathrm{d} + \alpha_\mathrm{c}\mathbf{U}_\mathrm{c}$. Eq. (70) ensures the boundedness of the phase fraction in theory. In the context of the moments, m_3 should be bounded roughly in $[0, 1.91]$, as reported in Eq. (67). Unfortunately, the moment transport equations have the same boundedness problem as of the $\nabla \cdot \mathbf{U}_\mathrm{d} \neq 0$ in Eq. (60). Buffo et al. [186] were inspired by Weller [185] to reformulate the moment transport equations as follows:

$$\frac{\partial m_k}{\partial t} + \nabla \cdot (\mathbf{U} m_k) - \nabla \cdot (\mathbf{U}_\mathrm{r} (1 - \alpha_\mathrm{d}) m_k) = 0. \tag{71}$$

It was proven that Eq. (71) ensure the boundedness of the moments [186]. However, the practical numerical procedure has limitations as well:

1) Eq. (71) can only utilize the first-order scheme because of the realizability problems which will be discussed in the next section. If a higher-order scheme was employed for Eq. (70), and a first order scheme was employed for Eq. (71) separately, the predict α_d and $\frac{\pi}{6} m_3$ will be different.
2) The strictly boundedness between 0 and 1 still can not be ensured by Eq. (70) due to its non-linear dependence on α_d as shown in the third term. A slightly negative value of α_d introduces divergence of the simulations. One possible solution is to solve the equation for α_d and α_c iteratively in each time step. However, it is computational demanding. Another practical solution is to employ the explicit Flux-correct transport (FCT) algorithm to solve Eq. (70), the variation of which was firstly implemented by OpenFOAM foundation in OpenFOAM-1.4.1 for the phase fraction equation. Therefore, it is reasonable to employ the FCT algorithm for the moment transport equations as reported in Eq. (71). However, due to the anti-diffusion procedure in FCT [187], it might introduce the realizability problems. Such numerical procedure needs further investigation.

B. Higher-order scheme and realizability

When a higher-order scheme is employed for the advection term, Eq. (71) tends to diverge. This problem is called the moment realizability problem or the moment corruption problem in the field of PBM. From the aspect of CFD, the realizability refers to the solution of a problem being physically realistic [188]. Algorithms that are not realizable may result in non-physical solutions or cause numerical methods to diverge. In the context of the QBMM, whenever the moment set corresponds to a non-negative NDF, the moment set is realizable. Unfortunately, the realizability of the moment set has been proven to be difficult to maintain by many works when the PBE is coupled with CFD for inhomogeneous systems [116], [189]–[192]. This non-realizable moments set is called the "invalid moment sets" [189]. If the invalid moment set were fed into the moment inversion algorithm, unrealizable abscissas would be calculated (e.g., $d < 0$), thereby jeopardizing the stability of the simulation. The necessary and sufficient condition for the existence of a non-negative and unique NDF for a moment set is the non-negativity of the Hankel-Hadamard determinant [193]

$$\Delta_{k,l} = \begin{vmatrix} m_k & m_{k+1} & \dots & m_{k+1} \\ m_{k+1} & m_{k+2} & \dots & m_{k+l+1} \\ \vdots & \vdots & \vdots & \vdots \\ m_{k+l} & m_{k+l+1} & \dots & m_{k+l+l} \end{vmatrix} \geq 0. \tag{72}$$

When the Hankel-Hadamard determinant is negative, the moment sets are invalid. However, it is not reasonable to compute all the Hankel-Hadamard determinants in each time step. Laurent and Nguyen [192] proposed to check the positivity of the ζ_k which are parameters of the PD algorithm. When ζ_k is positive, realizability criterion is satisfied.

Different algorithms were developed in order to overcome the problem. The correction algorithm [189] employs the first three moments to calculate the three parameters of the

log-normal distribution function and calculate the entire set of the realizable moments. The adaptive Wheeler algorithm returns the largest possible set of weights and abscissas [128]. However, when the moment transport equations are coupled with the CFD, it does not make sense to correct the invalid moment sets in each time step when the higher-order scheme is employed, as this leads to moment corruption. Vikas et al. [194] developed a realizable higher-order finite volume scheme for the KE with an advection term, and it was lately extended by Vikas et al. [191] to the PBE with a diffusion term. This scheme was based on the kinetics-based finite volume method (KBFVM) [73] since it was originally developed for the KE. However, the KBFVM is also applicable to the PBE. In the following, the higher-order scheme proposed by Vikas et al. [194] is called Vikas scheme.

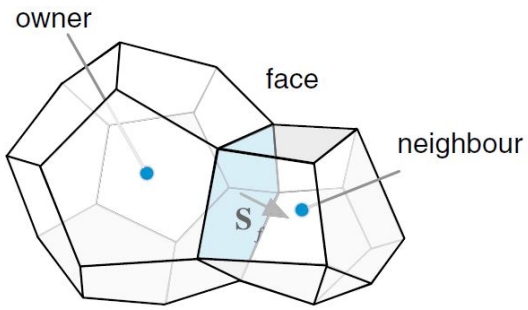

Fig. 5: The computational cell labelled by "owner" and "neighbour" in the unstructured computational mesh framework.

For the unstructured computational mesh, as reported in Fig.5, the NDF transport equations with constant dispersed velocity $\mathbf{U}_\mathrm{d}$ can be written as

$$\frac{\partial n}{\partial t} + \nabla \cdot (\mathbf{U}_\mathrm{d} n) = 0. \tag{73}$$

The source terms are neglected since they do not create non-realizability problems. If an explicit Euler time scheme is used with the finite volume method, the updated NDF for grid labelled by "own" for the time step $t + \Delta t$ can be calculated by

$$n_\mathrm{own}^{t+\Delta t} = n_\mathrm{own}^{t} - \lambda \sum_f F_f^t n_f^t, \tag{74}$$

where n_own and n_nei is the NDF for the owner grid and the neighbour grid, respectively; λ equals $\frac{\Delta t}{\Delta V_\mathrm{own}}$, in which Δt is the time step, V_own is the mesh volume; F_f^t and n_f^n is the flow flux and the NDF defined at the cell face "f" at time step t. If a first-order upwind scheme is applied, the n_f^t can be inferred from the upwind cell's value:

$$n_f^t = \begin{cases} n_\mathrm{own}^t, & F_f^t > 0 \\ n_\mathrm{nei}^t, & F_f^t < 0 \end{cases} \tag{75}$$

Substituting Eq. (75) into Eq. (74) yields

$$\begin{aligned} & n_\mathrm{own}^{t+\Delta t} \\ & = n_\mathrm{own}^t - \lambda \sum \max\left(F_f^t, 0\right) n_\mathrm{own}^t - \lambda \min\left(F_f^t, 0\right) n_\mathrm{nei}^t \\ & = \left(1 - \lambda \sum_f \max\left(F_f^t, 0\right)\right) n_\mathrm{own}^t - \lambda \sum_f \min\left(F_f^t, 0\right) n_\mathrm{nei}^t \end{aligned} \tag{76}$$

It can be seen that the last term in the R.H.S. of Eq. (76) is non-negative. If

$$\Delta t \leqslant \min\left(\frac{\Delta V_\mathrm{own}}{\sum_f \max\left(F_f^t, 0\right)}\right) \tag{77}$$

and the given initial NDF is non-negative, the NDF calculated by Eq. (76) will be always non-negative. This concludes the proof that when a first-order upwind scheme is employed for the PBE with an advection term, the reliability problem disappears when the CFL condition is satisfied, as reported in Eq. (77). The grouping procedure for the first two terms in the R.H.S of Eq. (76) is essential to solve the realizability problem and it forms the basis of the Vikas scheme [73], [194].

When a higher-order scheme is employed, Eq. (76) does not hold and it can not be simplified by grouping. However, if we substitute Eq. (23) into Eq. (73), it leads to

$$\begin{aligned} n_\mathrm{own}^{t+\Delta t} = & \sum_{\alpha=1}^{N} w_{\alpha,\mathrm{own}}^t \delta(d - d_{\alpha,\mathrm{own}})^t \\ & - \lambda \sum_f F_f^t \left(\sum_{\alpha=1}^{N} w_{\alpha,f}^t \delta(d - d_{\alpha,f})^t\right). \end{aligned} \tag{78}$$

By virtue of the KBFVM, the weights and abscissas on the cell face f are split as follows:

$$\begin{aligned} & F_f \sum_{\alpha=1}^{N} w_{\alpha,f}^t \delta(d - d_{\alpha,f})^t \\ & = \sum_{\alpha=1}^{N} \max(F_{f_\mathrm{own}}, 0) w_{\alpha,f_\mathrm{own}}^t \delta(d - d_{\alpha,f_\mathrm{own}})^t \\ & \quad + \sum_{\alpha=1}^{N} \min(F_{f_\mathrm{nei}}, 0) w_{\alpha,f_\mathrm{nei}}^t \delta(d - d_{\alpha,f_\mathrm{nei}})^t. \end{aligned} \tag{79}$$

Substituting Eq. (79) into Eq. (78) yields

$$\begin{aligned} n_\mathrm{own}^{t+\Delta t} = & \sum_{\alpha=1}^{N} w_{\alpha,\mathrm{own}}^t \delta(d - d_{\alpha,\mathrm{own}})^t \\ & - \lambda \sum_{\alpha=1}^{N} \sum_f \max(F_{f_\mathrm{own}}, 0) w_{\alpha,f_\mathrm{own}}^t \delta(d - d_{\alpha,f_\mathrm{own}})^t \\ & - \lambda \sum_{\alpha=1}^{N} \sum_f \min(F_{f_\mathrm{nei}}, 0) w_{\alpha,f_\mathrm{nei}}^t \delta(d - d_{\alpha,f_\mathrm{nei}})^t. \end{aligned} \tag{80}$$

The essence of the Vikas scheme is to employ the first-order spatial scheme for the abscissas and a higher-order scheme for

the weights. Therefore, the abscissas on the cell face can be approximated by

$$d_{\alpha.f_{\text{own}}} = d_{\alpha,\text{own}}, d_{\alpha.f_{\text{nei}}} = d_{\alpha,\text{nei}} \tag{81}$$

Substituting Eq. (81) into Eq. (80) yields

$$\begin{aligned} n_{\text{own}}^{t+\Delta t} = \\ \sum_{\alpha=1}^{N} \delta(d-d_{\alpha,\text{own}})^t \left(w_{\alpha,\text{own}}^t - \lambda \sum_f w_{\alpha,f_{\text{own}}}^t \max\left(F_{f_{\text{own}}}^t, 0\right) \right) \\ - \lambda \sum_{\alpha=1}^{N} \sum_f \min(F_{f_{\text{nei}}}, 0) w_{\alpha,f_{\text{nei}}}^t \delta(d - d_{\alpha,f_{\text{nei}}})^t. \end{aligned} \tag{82}$$

For any Δt that satisfies the condition

$$\Delta t \leqslant \min_{\text{own},\alpha} \left(\frac{w_{\alpha,\text{own}}^t \Delta V_{\text{own}}}{\sum_f w_{\alpha,f_{\text{own}}}^t \max\left(F_{f_{\text{own}}}^t, 0\right)} \right) \tag{83}$$

the NDF is non-negative. It can be seen that in the Vikas scheme, if the first-order scheme is applied to the abscissas and the discritized time step satisfies Eq. (83), a higher-order scheme for the weights can be employed to prevent the moment realizability problem in the Euler explicit time marching scheme. It is straightforward to extend the Vikas scheme to other problems, such as the PBE with diffusion terms [191]. Therefore, the discussion is omitted here for brevity.

Another explanation which is easier to understand the Vikas scheme is also briefly discussed here. The spirit of the Vikas scheme is to employed the monotonic upwind scheme for conservation laws (MUSCL) type of reconstruction on the canonical moments flux at the grid interface, which is calculated by the piecewise linear (or polynomial) reconstruction of the weights and the piecewise constant reconstruction of other variables. As shown in Fig. 6, for a uniform grid (labelled by I) with spacing Δx, we have

$$\begin{cases} w_\beta^I(x) = w_\beta^I + \sigma_\beta^I(x - x^I) \\ d_\beta^I(x) = d_\beta^I \end{cases}, x^I - \frac{\Delta x}{2} \leq x \leq x^I + \frac{\Delta x}{2}, \tag{84}$$

where σ_β^I is the slope on the Ith cell. Substituting Eq. (84) into Eq. (13), it leads to

$$m_k^I(x) = \sum_{\beta=1}^{N} \left(w_\beta^I + \sigma_\beta^I(x - x^I)\right) \left(d_\beta^I\right)^k. \tag{85}$$

It can be seen that $m_k^I(x)$, at any location x, satisfy Eq. (13) itself for any slope σ_β^I and these moments values are ensured to be realizable. In the following we use the 1-D equation

$$\frac{\partial m_k}{\partial t} + u \frac{\partial m_k}{\partial t} = 0 \tag{86}$$

and the piecewise linear reconstruction of weights as an example to show the procedure of Vikas scheme. It can be divided into two main steps:

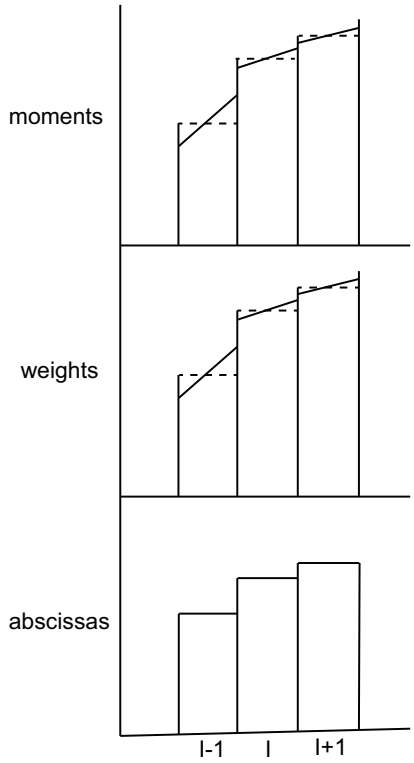

Fig. 6: Piecewise linear reconstruction of the moments, weights and constant reconstruction for the abscissas.

1) Discretize Eq. (86) by explicit time-marching scheme:

$$M_k^{I,t+\Delta t} = M_k^I - \frac{\Delta t}{\Delta x} \left(F^{I+1/2} - F^{I-1/2}\right), \tag{87}$$

where $M_{k,}^{I,t+\Delta t}$ is the average value of m_k over the Ith grid at $t+\Delta t$, $F^{I+1/2}$ and $F^{I-1/2}$ are the moments flux functions defined at the interface $I+1/2$ and $I-1/2$ for Ith grid, respectively.

2) Instead of interpolating the flux from the moments, Vikas scheme calculates from the weights and abscissas as the following:

$$\begin{aligned} F^{I+1/2} = \sum_{\beta=1}^{N} \max(u_\beta^I, 0) \Delta S \left(w_\beta^I + \sigma_\beta^I \frac{\Delta x}{2}\right) \left(d_\beta^I\right)^i \\ + \sum_{\beta=1}^{N} \min(u_\beta^{I+1}, 0) \Delta S \left(w_\beta^{I+1} - \sigma_\beta^{I+1} \frac{\Delta x}{2}\right) \left(d_\beta^{I+1}\right)^i, \end{aligned} \tag{88}$$

where $\Delta S = \Delta y \Delta z$, which is the grid interface surface normal to x-plane. The flux calculation corresponds to the flux-vector splitting procedure: the first term in the R.H.S of Eq. (88) denotes the particles moving from the Ith grid crossing the $I+1/2$ interface, whereas the second denotes the particles moving from the $I+1$th grid crossing the $I+1/2$ interface. The flux at $I-1/2$ can be calculated by similar way.

Readers may find the Vikas scheme is only 1st-order accurate in time. Following the spirit of total variation diminishing (TVD) time stepping, multi-stage explicit time-integration schemes can be used in practice to obtain a higher-order time scheme (the subscript are omitted for brevity):

$$\begin{aligned} m^* &= m + F(m), \\ m^{**} &= m^* + F(m^*), \\ m^{t+\Delta t} &= \frac{1}{2}\left(m^* + m^{**}\right), \end{aligned} \tag{89}$$

where F is the flux function. It can be easily proven that the two-stage second-order Runge-Kutta method combined the flux calculation based on Vikas scheme, as reported equations above, can ensure moments realizability. However, numerical problems still exist as discussed as follows:

1) The numerical treatment of the moments are important when the dispersed phase disappears. This phenomenon is called phase segregation in multiphase flow field. For example, in the bubble columns simulations, the initial bubble column is often filled by water, which implies α_{d} and the kth order moment is theoretically zero due to the absence of bubbles. However, such numerical challenging settings introduce numerical problems for the TFM and QBMMs. In TFM, it leads to the singular problem which can be prevented by numerical manipulation on the source term. In such cases, the "disappeared" phase's velocity equals the terminal velocity. In QBMMs, the phase segragation implies the weights are zero in these computational cells. According to Eq. (83), it implies the time step tends to zero. Otherwise the advected moments will be un-realizable. One possible solution would be setting the initial moments to be a relative small value [158]. Such numerical treatment needs further investigations and verifications.
2) The Vikas scheme is suitable for Eq. (73). It was proven by Buffo et al. [186] that it introduces unbounded solutions. In order to ensure the boundedness, one possible solution is to employ Vikas scheme to solve Eq. (71), in which two advection terms exist. Meanwhile, the prediction of the m_3 should be identical with α_{d} if the TFM was employed to simulate two-phase flows. However, the agreement of m_3 and α_{d} can be only obtained by applying identical numerical scheme to these variables. The possible solution is to combine the FCT algorithm and Vikas scheme for the moment transport equations to ensure boundedness. Such numerical treatment needs further investigations and verifications.

It should be noted here that the higher-order Vikas scheme was called "quasi-second-order" scheme by Laurent and Nguyen [192], as of the higher-order scheme can not be employed for the weights. Other higher-order schemes were proposed by them which were called ζ scheme, ζ simplified scheme, QW scheme and QW simplified scheme. These schemes are based on the calculation of ζ which can be calculated by the moment inversion algorithm (e.g. PD algorithm). The simplified schemes were also developed under the KBFVM framework, and the ζ simplified scheme was recently implemented in the OpenQBMM [179]. The QW simplified scheme shares large similarities with the Vikas scheme, but the interpolation of weights and abscissas to cell faces are omitted. The key difference lies in that the CFL number for ζ simplified scheme and QW simplified scheme should be smaller than $1/3$ and $1/2$, respectively. Readers who are interested in this scheme are referred to their latest work [192]. Benchmark test cases of ζ based schemes need to be investigated in the future.

C. Reconstructed NDF

All the QBMMs track the moments instead of the NDF, which implies that the information of the rigorous NDF can not be directly provided by the algorithm. The algorithm works well for breakage and coalescence dominated processes and other similar processes where only the information of the mean Sauter diameter is required. However, in certain cases it introduces problems. For example, in evaporation simulations, it leads to a zero-order moment equation that contains a term that corresponds to the loss of particles of zero size. In order to evaluate this term, the value of the NDF at $d = 0$ is required but is not available in the QMOM or the DQMOM. When the NDF was employed in LES framework, the velocity dispersion around the velocity abscissas are also necessary. A possible solution is to increase the number of abscissas to a large enough value (e.g., $N > 100$), such that the smallest abscissa's expected value tends to zero. However, it was proven that the moment inversion algorithm is not accurate for N larger than approximately 10 [123], [195]. In some works, it is even proven that these methods suffer from ill conditioning if $N > 3$ [133], [190], [196]. Thus, the QMOM and the DQMOM can not be employed for certain problems.

The NDF can be calculated from the moments if the NDF is defined a-prior. For example, if the NDF is expressed as

$$n = \exp\left(\sum_{i=1}^{N} A_i L^i\right), \tag{90}$$

where A_i is the unknown coefficients. The corresponding moments can be written as

$$m_k = \int d^k \exp\left(\sum_{i=1}^{N} A_i d^i\right). \tag{91}$$

Given N moments, the coefficients A_i can be found by Newton-Raphson method to reconstruct the NDF. Such method was adapted for crystallization problems [197]. The EQMOM follows similar idea. In theory, the reconstructed NDF that is predicted by the EQMOM will overlap with the shape of the real NDF since the parameters of the KDF can be calculated analytically. However, because the values of σ are often assumed to be identical in Eq. (33) to avoid the nonlinear solver, error will be introduced if two or more primary nodes are employed. When the NDF is reconstructed from the moments, possible problems are listed as follows:

1) If the real NDF is assumed by summation of the KDF with different values of σ, the predicted reconstructed

NDF by the EQMOM will deviate from the original NDF [165], [170].

2) When many primary nodes are employed, as reported in Fig. 7, the reconstructed NDF show oscillations, which originate from the summation of the KDF [165], [170].
3) The reconstructed NDF that is predicted by the EQMOM is highly dependent on the shape of the KDF. It can be seen in Fig. 7 that if the log-normal EQMOM is employed to predict the real NDF with a beta distribution shape, it will fail because the left tail of the log-normal distribution tends to zero, which is not the case for the beta distribution function. Similar problems were reported in the works by [129], [165], [170], [198]

However, it should be stress there that although the reconstructed NDF that is calculated from the moments may deviate from the accurate NDF, this does not affect the stability of the numerical simulation. Moreover, the predicted moments are consistent.

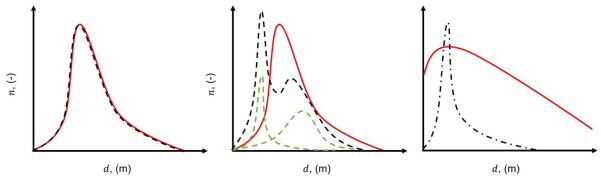

Fig. 7: Left: comparison of the real NDF (solid red line) with the log-normal shape and the reconstructed NDF by the log-normal EQMOM with one primary node (dashed black line). Middle: comparison of the real NDF (solid red line) with the log-normal shape and the reconstructed NDF by the log-normal EQMOM with two primary nodes (dashed black line). The dashed green lines represent the reconstructed NDF by each primary node. Right: comparison of the real NDF (solid red line) with the beta distribution shape and the reconstructed NDF by the log-normal EQMOM with one primary node (dashed black line).

V. Conclusions

The PBE can be employed to model the dispersed phase in multiphase flows. The analytical solution of the PBE can be only obtained under rigid assumptions. A large variety of algorithms for solving the PBE have been developed. Among them, the QBMMs were proven to be efficient, especially when the PBE was coupled with CFD simulations for multiphase flows. Over the years, the QMOM, DQMOM, CQMOM, EQMOM, ECQMOM, and HyQMOM were developed for different problems, and each has advantages and drawbacks. In the present work, the algorithms of these QBMMs for spatially homogeneous systems with first-order and second-order point processes was comprehensively studied. The numerical aspects when the QBMM was coupled with CFD for inhomogeneous multiphase systems were investigated. The limitations of each algorithm were also discussed. The boundedness problem and the realizability problem of the moment sets when a higher-order scheme was employed were presented and possible solutions were summarized.

The numerical challenges and the limitations of the QBMM are clear and further studies on a more robust and efficient algorithm are indispensable. Ideally, a quadrature-based moment algorithm should be able to provide a non-negative NDF accurately within the internal coordinate limits without the realizability problem. The spatial numerical scheme should ensure the boundedness of the moments. In addition, the algorithm should be able to capture the mathematical characteristics of the equations to be solved.

In the future, the algorithm of the coupling between the CFD and the generalized population balance equation (GPBE) will be reviewed.

Acknowledgements

This work is the updated version of our previous work (see [199]). Dongyue Li wants to acknowledge Prof. Daniele Marchisio for shedding light on the QBMM. He also wants to acknowledge the small, but active, CFD community in China (cfd-china.com) for all their continued encouragement.

Appendix A. A concrete example of initial moments calculation

QBMM starts the iteration from the initial moments. These moments represent statistical features of the NDF. In order to calculate realizable moments, an initial NDF should be assumed. For diameter-based NDF, it is common to assume a log-normal distribution function:

$$n(d) \approx \frac{1}{d\sigma\sqrt{2\pi}} \exp\left(-\frac{(\ln d - \mu)^2}{2\sigma^2}\right), \tag{92}$$

where σ and μ are the log-normal distribution parameters which can be computed by

$$\mu = \ln\left(\frac{m^2}{\sqrt{v+m^2}}\right), \tag{93}$$

$$\sigma = \sqrt{\ln\left(\frac{v}{m^2}+1\right)}, \tag{94}$$

where m is the mean value, $\sqrt{v}$ is the dtandard deviation. The initial raw moments based on the log-normal NDF can be expressed as follows:

$$m_k = N \exp\left(k\mu + \frac{k^2\sigma^2}{2}\right), \tag{95}$$

where N is the number of particles in per unit, which can be calculated from the given phase fraction as follows:

$$N = \frac{\alpha_{\mathrm{d}}}{k_v \exp\left(3\mu + \frac{3^2\sigma^2}{2}\right))}, \tag{96}$$

where k_v is the shape parameter equals $\pi/6$. In practice, m can be seen as the mean particle diameter (e.g., mean Sauter diameter), $\sqrt{v}$ can be set equal to a small value (e.g., 15 %). Since the moments are calculated from the NDF, they are ensured to be realizable.

Another simpler approach can be used. One can calculate the initial moments directly from the weights and abscissas as reported in Eq. (13). The summation of weights should be equal to N. For example, if three nodes QMOM is used, one can assume $w_1 = 500$, $w_2 = 600$, $w_3 = 700$, $d_1 = 0.005$, $d_2 = 0.006$ and $d_3 = 0.007$. The moments can be calculated by $m_k = \sum w_i d_i^k$. In this approach, the presumed NDF's shape can be hardly obtained. It should be stressed that d_i cannot be identical, otherwise the moments cannot be realizable.

Appendix B. Dimension of the moments

The dimension of the moments is dependent on the number density function. If the internal coordinate is particle diameter d, the dimension of the number density function $n(d)$ is 1/m^4. Therefore, the dimension of kth moments of $n(d)$ is m^{-3}, m^{-2}, m^{-1}, m^0,..., m^{k-3}. If the internal coordinate is particle volume V, the dimension of the number density function $n(V)$ is 1/m^{-6}. The dimension of kth moments of $n(V)$ is m^{-3}, m^0, m^3, m^6,..., m^{k-3}. It should be noted that the weights' dimension is m^{-3}. Meanwhile, it can be seen that the m_3 for $n(d)$ and m_1 for $n(V)$ is dimensionless, which can be related to the phase fraction α by the shape factor.

References

[1] V. Buwa, V. Ranade, Dynamics of gas–liquid flow in a rectangular bubble column: experiments and single/multi-group CFD simulations, Chemical Engineering Science 57 (2002) 4715–4736.

[2] T. Wang, J. Wang, Y. Jin, Population balance model for gas- liquid flows: Influence of bubble coalescence and breakup models, Industrial & Engineering Chemistry Research 44 (2005) 7540–7549.

[3] M. Laakkonen, V. Alopaeus, J. Aittamaa, Validation of bubble breakage, coalescence and mass transfer models for gas–liquid dispersion in agitated vessel, Chemical Engineering Science 61 (2006) 218–228.

[4] M. Bhole, J. Joshi, D. Ramkrishna, CFD simulation of bubble columns incorporating population balance modeling, Chemical Engineering Science 63 (2008) 2267–2282.

[5] A. Buffo, D. Marchisio, M. Vanni, P. Renze, Simulation of coalescence, break up and mass transfer in gas-liquid systems by using monte carlo and quadrature-based moment methods, in: Ninth International Conference on CFD in the Minerals and Process Industries, 2012.

[6] A. Buffo, M. Vanni, D. Marchisio, R. Fox, Multivariate quadrature-based moments methods for turbulent polydisperse gas–liquid systems, International Journal of Multiphase Flow 50 (2013) 41–57.

[7] Y. Liao, D. Lucas, E. Krepper, Application of new closure models for bubble coalescence and breakup to steam–water vertical pipe flow, Nuclear Engineering and Design 279 (2014) 126–136.

[8] Y. Liao, D. Lucas, Poly-disperse simulation of condensing steam-water flow inside a large vertical pipe, International Journal of Thermal Sciences 104 (2016) 194–207.

[9] A. Buffo, M. Vanni, P. Renze, D. Marchisio, Empirical drag closure for polydisperse gas–liquid systems in bubbly flow regime: Bubble swarm and micro-scale turbulence, Chemical Engineering Research and Design 113 (2016) 284–303.

[10] X. Liang, H. Pan, Y. Su, Z. Luo, CFD-PBM approach with modified drag model for the gas–liquid flow in a bubble column, Chemical Engineering Research and Design 112 (2016) 88–102.

[11] H. Pan, X. Chen, X. Liang, L. Zhu, Z. Luo, CFD simulations of gas-liquid-solid flow in fluidized bed reactors-A review, Powder Technology 299 (2016) 235–258.

[12] D. Cheng, S. Wang, C. Yang, Z. Mao, Numerical simulation of turbulent flow and mixing in Gas-Liquid-Liquid stirred tanks, Industrial & Engineering Chemistry Research 56 (2017) 13050—-13063.

[13] K. Guo, T. Wang, Y. Liu, J. Wang, CFD-PBM simulations of a bubble column with different liquid properties, Chemical Engineering Journal 329 (2017) 116–127.

[14] G. Yang, K. Guo, T. Wang, Numerical simulation of the bubble column at elevated pressure with a CFD-PBM coupled model, Chemical Engineering Science 170 (2017) 251–262.

[15] M. Jaradat, M. Attarakih, H. Bart, Effect of phase dispersion and mass transfer direction on steady state RDC performance using population balance modelling, Chemical Engineering Journal 165 (2010) 379–387.

[16] V. Alopaeus, Analysis of concentration polydispersity in mixed liquid–liquid systems, Chemical Engineering Research and Design 92 (2014) 612–618.

[17] J. Mitre, P. Lage, M. Souza, E. Silva, L. Barca, A. Moraes, R. Coutinho, E. Fonseca, Droplet breakage and coalescence models for the flow of water-in-oil emulsions through a valve-like element, Chemical Engineering Research and Design 92 (2014) 2493–2508.

[18] M. Attarakih, S. Alzyod, M. Hlawitschke, H. Bart, OPOSSIM: a population balance-SIMULINK module for modelling coupled hydrodynamics and mass transfer in liquid extraction equipment, Computer Aided Chemical Engineering 37 (2015) 257–262.

[19] J. Favero, L. Silva, P. Lage, Modeling and simulation of mixing in water-in-oil emulsion flow through a valve-like element using a population balance model, Computers & Chemical Engineering 75 (2015) 155–170.

[20] A. Buffo, V. Alopaeus, Solution of bivariate population balance equations with high-order moment-conserving method of classes, Computers & Chemical Engineering 87 (2016) 111–124.

[21] Z. Gao, D. Li, A. Buffo, W. Podgórska, D. Marchisio, Simulation of droplet breakage in turbulent liquid–liquid dispersions with CFD-PBM: Comparison of breakage kernels, Chemical Engineering Science 142 (2016) 277–288.

[22] A. Bourdillon, P. Verdin, C. Thompson, Numerical simulations of drop size evolution in a horizontal pipeline, International Journal of Multiphase Flow 78 (2016) 44–58.

[23] D. Li, A. Buffo, W. Podgórska, Z. Gao, D. Marchisio, Droplet breakage and coalescence in liquid-liquid dispersions: comparison of different kernels with EQMOM and QMOM, AIChE Journal 63 (2017) 2293–2311.

[24] D. Li, A. Buffo, W. Podgórska, D. Marchisio, Z. Gao, Investigation of droplet breakup in liquid-liquid dispersions by CFD-PBM simulations: The influence of the surfactant type, Chinese Journal of Chemical Engineering 25 (2017) 1369–1380.

[25] S. Alzyod, M. Attarakih, A. Hasseine, H. Bart, Steady state modeling of Kühni liquid extraction column using the Spatially Mixed Sectional Quadrature Method of Moments (SM-SQMOM), Chemical Engineering Research and Design 117 (2017) 549–556.

[26] A. Misra, L. De Souza, M. Illner, L. Hohl, M. Kraume, J. Repke, D. Thévenin, Simulating separation of a multiphase liquid-liquid system in a horizontal settler by CFD, Chemical Engineering Science 167 (2017) 242–250.

[27] C. Qin, C. Chen, Q. Xiao, N. Yang, C. Yuan, C. Kunkelmann, M. Cetinkaya, K. Mülheims, CFD-PBM simulation of droplets size distribution in rotor-stator mixing devices, Chemical Engineering Science 155 (2016) 16–26.

[28] L. Xie, Q. Liu, Z. Luo, A multiscale CFD-PBM coupled model for the kinetics and liquid–liquid dispersion behavior in a suspension polymerization stirred tank, Chemical Engineering Research and Design 130 (2018) 1–17.

[29] R. Fox, F. Laurent, M. Massot, Numerical simulation of spray coalescence in an Eulerian framework: direct quadrature method of moments and multi-fluid method, Journal of Computational Physics 227 (2008) 3058–3088.

[30] R. Fox, A quadrature-based third-order moment method for dilute gas-particle flows, Journal of Computational Physics 227 (2008) 6313–6350.

[31] O. Desjardins, R. Fox, P. Villedieu, A quadrature-based moment method for dilute fluid-particle flows, Journal of Computational Physics 227 (2008) 2514–2539.

[32] A. Passalacqua, R. Fox, Implementation of an iterative solution procedure for multi-fluid gas–particle flow models on unstructured grids, Powder Technology 213 (2011) 174–187.

[33] W. Yan, J. Li, Z. Luo, A CFD-PBM coupled model with polymerization kinetics for multizone circulating polymerization reactors, Powder Technology 231 (2012) 77–87.

[34] M. Hussain, M. Peglow, E. Tsotsas, J. Kumar, Modeling of aggregation kernel using monte carlo simulations of spray fluidized bed agglomeration, AIChE Journal 60 (2014) 855–868.

[35] W. Yan, Z. Luo, Y. Lu, X. Chen, A CFD-PBM-PMLM integrated model for the gas–solid flow fields in fluidized bed polymerization reactors, AIChE Journal 58 (2012) 1717–1732.

[36] M. Hussain, J. Kumar, E. Tsotsas, Micro-Macro transition of population balances in fluidized bed granulation, Procedia Engineering 102 (2015) 1399–1407.

[37] Y. Yao, J. Su, Z. Luo, CFD-PBM modeling polydisperse polymerization FBRs with simultaneous particle growth and aggregation: the effect of the method of moments, Powder Technology 272 (2015) 142–152.

[38] T. Nguyen, F. Laurent, R. Fox, M. Massot, Solution of population balance equations in applications with fine particles: mathematical modeling and numerical schemes, Journal of Computational Physics 325 (2016) 129–156.

[39] E. Ghadirian, J. Abbasian, H. Arastoopour, CFD simulation of particle size change during the coal char gasification process using the population balance model with FCMOM, Powder Technology 323 (2017) 128–138.

[40] B. Kong, R. Fox, A solution algorithm for fluid–particle flows across all flow regimes, Journal of Computational Physics 344 (2017) 575–594.

[41] B. Kong, R. Fox, H. Feng, J. Capecelatro, R. Patel, O. Desjardins, Euler–euler anisotropic gaussian mesoscale simulation of homogeneous cluster-induced gas–particle turbulence, AIChE Journal 63 (2017) 2630–2643.

[42] S. Shekar, A. Smith, W. Menz, M. Sander, M. Kraft, A multidimensional population balance model to describe the aerosol synthesis of silica nanoparticles, Journal of Aerosol Science 44 (2012) 83–98.

[43] R. Guichard, A. Tanière, E. Belut, N. Rimbert, Simulation of nanoparticle coagulation under brownian motion and turbulence in a differential–algebraic framework: Developments and applications, International Journal of Multiphase Flow 64 (2014) 73–84.

[44] M. Yu, J. Lin, Hybrid method of moments with interpolation closure–Taylor-series expansion method of moments scheme for solving the Smoluchowski coagulation equation, Applied Mathematical Modelling 52 (2017) 94–106.

[45] M. Yu, Y. Liu, A. Koivisto, An efficient algorithm scheme for implementing the TEMOM for resolving aerosol dynamics, Aerosol Science and Engineering 1 (2017) 119–137.

[46] P. Marchal, R. David, J. Klein, J. Villermaux, Crystallization and precipitation engineering-I. An efficient method for solving population balance in crystallization with agglomeration, Chemical Engineering Science 43 (1988) 59–67.

[47] F. Puel, G. Fevotte, J. Klein, Simulation and analysis of industrial crystallization processes through multidimensional population balance equations. Part 1: a resolution algorithm based on the method of classes, Chemical Engineering Science 58 (2003) 3715–3727.

[48] S. Qamar, G. Warnecke, Numerical solution of population balance equations for nucleation, growth and aggregation processes, Computers & Chemical Engineering 31 (2007) 1576–1589.

[49] B. Balakin, A. Hoffmann, P. Kosinski, Population balance model for nucleation, growth, aggregation, and breakage of hydrate particles in turbulent flow, AIChE Journal 56 (2010) 2052–2062.

[50] A. Majumder, V. Kariwala, S. Ansumali, A. Rajendran, Lattice boltzmann method for population balance equations with simultaneous growth, nucleation, aggregation and breakage, Chemical Engineering Science 69 (2012) 316–328.

[51] S. Cheung, L. Deju, G. Yeoh, J. Tu, Modeling of bubble size distribution in isothermal gas–liquid flows: Numerical assessment of population balance approaches, Nuclear Engineering and Design 265 (2013) 120–136.

[52] T. Vetter, M. Iggland, D. Ochsenbein, F. Hänseler, M. Mazzotti, Modeling nucleation, growth, and ostwald ripening in crystallization processes: a comparison between population balance and kinetic rate equation, Crystal Growth & Design 13 (2013) 4890–4905.

[53] A. Hasseine, H. Bart, A domian decomposition method solution of population balance equations for aggregation, nucleation, growth and breakup processes, Applied Mathematical Modelling 39 (2015) 1975–1984.

[54] J. Cheng, C. Yang, M. Jiang, Q. Li, Z. Mao, Simulation of antisolvent crystallization in impinging jets with coupled multiphase flow-micromixing-PBE, Chemical Engineering Science 171 (2017) 500–512.

[55] S. Rigopoulos, Population balance modelling of polydispersed particles in reactive flows, Progress in Energy and Combustion Science 36 (2010) 412–443.

[56] E. Abbasi, H. Arastoopour, Numerical simulation of CO2 removal process using solid sorbent in a fluidized bed: A CFD-PBE model, in: 2011 AIChE Annual Meeting, Minneapolis, USA, 2011.

[57] J. Akroyd, A. Smith, R. Shirley, L. McGlashan, M. Kraft, A coupled CFD-population balance approach for nanoparticle synthesis in turbulent reacting flows, Chemical Engineering Science 66 (2011) 3792–3805.

[58] E. Yapp, D. Chen, J. Akroyd, S. Mosbach, M. Kraft, J. Camacho, H. Wang, Numerical simulation and parametric sensitivity study of particle size distributions in a burner-stabilised stagnation flame, Combustion and Flame 162 (2015) 2569–2581.

[59] E. Abbasi, J. Abbasian, H. Arastoopour, CFD-PBE numerical simulation of CO2 capture using MgO-based sorbent, Powder Technology 286 (2015) 616–628.

[60] E. Yapp, C. Wells, J. Akroyd, S. Mosbach, R. Xu, M. Kraft, Modelling PAH curvature in laminar premixed flames using a detailed population balance model, Combustion and Flame 176 (2017) 172–180.

[61] A. Boje, J. Akroyd, S. Sutcliffe, J. Edwards, M. Kraft, Detailed population balance modelling of Tio2 synthesis in an industrial reactor, Chemical Engineering Science 164 (2017) 219–231.

[62] S. Mosbach, W. Menz, M. Kraft, Outlier analysis for a silicon nanoparticle population balance model, Combustion and Flame 177 (2017) 89–97.

[63] A. Zucca, D. Marchisio, A. Barresi, R. Fox, Implementation of the population balance equation in CFD codes for modelling soot formation in turbulent flames, Chemical Engineering Science 61 (2006) 87–95.

[64] D. Chen, Z. Zainuddin, E. Yapp, J. Akroyd, S. Mosbach, M. Kraft, A fully coupled simulation of PAH and soot growth with a population balance model, Proceedings of the Combustion Institute 34 (2013) 1827–1835.

[65] B. Wang, S. Mosbach, S. Schmutzhard, S. Shuai, Y. Huang, M. Kraft, Modelling soot formation from wall films in a gasoline direct injection engine using a detailed population balance model, Applied Energy 163 (2016) 154–166.

[66] F. Laurent, M. Massot, Multi-fluid modelling of laminar poly-disperse spray flames: origin, assumptions and comparison of sectional and sampling methods, Combustion theory and modelling 5 (2001) 537–572.

[67] O. Emre, R. Fox, M. Massot, S. De Chaisemartin, S. Jay, F. Laurent, Towards eulerian modeling of a polydisperse evaporating spray under realistic internal-combustion-engine conditions, Flow, turbulence and combustion 93 (2014) 689–722.

[68] M. Hussain, J. Kumar, E. Tsotsas, A new framework for population balance modeling of spray fluidized bed agglomeration, Particuology 19 (2015) 141–154.

[69] D. Kah, O. Emre, Q. Tran, S. De Chaisemartin, S. Jay, F. Laurent, M. Massot, High order moment method for polydisperse evaporating sprays with mesh movement: application to internal combustion engines, International Journal of Multiphase Flow 71 (2015) 38–65.

[70] M. Essadki, S. De Chaisemartin, M. Massot, F. Laurent, A. Larat, S. Jay, A new high order moment method for polydisperse evaporating sprays dedicated to the coupling with separated two-phase flows in automotive engine, in: 9th International Conference on Multiphase Flow (ICMF), 2016.

[71] M. Essadki, S. De Chaisemartin, F. Laurent, M. Massot, High order moment model for polydisperse evaporating sprays towards interfacial geometry, arXiv preprint arXiv:1608.07148 (2016).

[72] A. Sibra, J. Dupays, A. Murrone, F. Laurent, M. Massot, Simulation of reactive polydisperse sprays strongly coupled to unsteady flows in solid rocket motors: Efficient strategy using Eulerian Multi-Fluid methods, Journal of Computational Physics 339 (2017) 210–246.

[73] D. Marchisio, R. Fox, Computational models for polydisperse particulate and multiphase systems, Cambridge University Press, 2013.

[74] D. Ramkrishna, M. Singh, Population balance modeling: current status and future prospects, Annual review of chemical and biomolecular engineering 5 (2014) 123–146.

[75] J. Solsvik, H. Jakobsen, The foundation of the population balance equation: a review, Journal of Dispersion Science and Technology 36 (2015) 510–520.

[76] H. Arastoopour, D. Gidaspow, E. Abbasi, Computational Transport Phenomena of Fluid-Particle Systems, Springer, 2017.

[77] D. Ramkrishna, Population balances: Theory and applications to particulate systems in engineering, Academic Press, 2000.

[78] P. Lage, Comments on the "An analytical solution to the population balance equation with coalescence and breakage—the special case with constant number of particle" by D.P. Patil. and J.R.G. Andrews. [Chemical Engineering Science 53 (3) 599–601], Chemical Engineering Science 57 (2002) 4253–4254.

[79] B. McCoy, G. Madras, Analytical solution for a population balance equation with aggregation and fragmentation, Chemical Engineering Science 58 (2003) 3049–3051.

[80] G. Bhutani, P. Brito-Parada, Analytical solution for a three-dimensional non-homogeneous bivariate population balance equation—a special case, International Journal of Multiphase Flow 89 (2017) 413–416.

[81] M. Attarakih, A. Hasseine, H. Bart, On the solution of the PBE by orthogonal expansion of the maximum entropy functional, Computer Aided Chemical Engineering 40 (2017) 2053–2058.

[82] S. Kumar, D. Ramkrishna, On the solution of population balance equations by discretization–III. Nucleation, growth and aggregation of particles, Chemical Engineering Science 52 (1997) 4659–4679.

[83] D. Jo, S. Revankar, Investigation of bubble breakup and coalescence in a packed-bed reactor–Part 1: A comparative study of bubble breakup and coalescence models, International Journal of Multiphase Flow 37 (2011) 995–1002.

[84] J. Morchain, M. Pigou, N. Lebaz, A population balance model for bioreactors combining interdivision time distributions and micromixing concepts, Biochemical Engineering Journal 126 (2017) 135–145.

[85] H. Hulburt, S. Katz, Some problems in particle technology: A statistical mechanical formulation, Chemical Engineering Science 19 (1964) 555–574.

[86] J. Brock, J. Oates, Moment simulation of aerosol evaporation, Journal of aerosol science 18 (1987) 59–64.

[87] X. Luo, Y. Cao, H. Xie, F. Qin, Moment method for unsteady flows with heterogeneous condensation, Computers & Fluids 146 (2017) 51–58.

[88] M. Nicmanis, M. Hounslow, Finite-element methods for steady-state population balance equations, AIChE Journal 44 (1998) 2258–2272.

[89] J. Solsvik, H. Jakobsen, Evaluation of weighted residual methods for the solution of a population balance model describing bubbly flows: The least-squares, galerkin, tau, and orthogonal collocation methods, Industrial and Engineering Chemistry Research 52 (2013) 15988–16013.

[90] J. Solsvik, P. Becker, N. Sheibat-Othman, H. Jakobsen, On the solution of the dynamic population balance model describing emulsification: Evaluation of weighted residual methods, The Canadian Journal of Chemical Engineering 92 (2014) 250–265.

[91] J. Solsvik, P. Becker, N. Sheibat-Othman, H. Jakobsen, Numerical solution of the drop population balance equation using weighted residual and finite volume methods, Journal of Dispersion Science and Technology 37 (2016) 80–88.

[92] M. Smith, T. Matsoukas, Constant-number Monte Carlo simulation of population balances, Chemical Engineering Science 53 (1998) 1777–1786.

[93] H. Zhao, A. Maisels, T. Matsoukas, C. Zheng, Analysis of four Monte Carlo methods for the solution of population balances in dispersed systems, Powder Technology 173 (2007) 38–50.

[94] Y. He, H. Zhao, H. Wang, C. Zheng, Differentially weighted direct simulation Monte Carlo method for particle collision in gas–solid flows, Particuology 21 (2015) 135–145.

[95] Z. Xu, H. Zhao, C. Zheng, Fast Monte Carlo simulation for particle coagulation in population balance, Journal of Aerosol Science 74 (2014) 11–25.

[96] P. Fede, O. Simonin, P. Villedieu, Monte-Carlo simulation of colliding particles or coalescing droplets transported by a turbulent flow in the framework of a joint fluid–particle pdf approach, International Journal of Multiphase Flow 74 (2015) 165–183.

[97] Z. Xu, H. Zhao, C. Zheng, Accelerating population balance–Monte Carlo simulation for coagulation dynamics from the Markov jump model, stochastic algorithm and GPU parallel computing, Journal of Computational Physics 281 (2015) 844–863.

[98] W. Zhang, C. You, Numerical approach to predict particle breakage in dense flows by coupling multiphase particle-in-cell and Monte Carlo methods, Powder Technology 283 (2015) 128–136.

[99] Z. Xu, H. Zhao, H. Zhao, CFD-population balance Monte Carlo simulation and numerical optimization for flame synthesis of TiO2 nanoparticles, Proceedings of the Combustion Institute 36 (2017) 1099–1108.

[100] H. Liu, T. Chan, Differentially weighted operator splitting Monte Carlo method for simulating complex aerosol dynamic processes, Particuology (2017) In Press.

[101] S. Liu, T. Chan, A coupled CFD-Monte Carlo method for simulating complex aerosol dynamics in turbulent flows, Aerosol Science and Technology 51 (2017) 269–281.

[102] A. Vikhansky, Direct quadrature spanning tree method for solution of the population balance equations, Journal of Aerosol Science 55 (2013) 78–88.

[103] G. Ferreira, P. Lage, L. Silva, Extension and convergence analysis of the univariate direct quadrature spanning tree method, Powder Technology 322 (2017) 301–313.

[104] P. Roache, Code verification by the method of manufactured solutions, Transactions-American Society of Mechanical Engineers Journal of Fluids Engineering 124 (2002) 4–10.

[105] J. Solsvik, H. Jakobsen, Spectral solution of the breakage–coalescence population balance equation Picard and Newton iteration methods, Applied Mathematical Modelling 40 (2016) 1741–1753.

[106] L. Schneider, N. Le Lostec, P. Villedieu, A. Sadiki, A moment method for splashing and evaporation processes of polydisperse sprays, International Journal of Multiphase Flow 36 (2010) 261–272.

[107] B. Lad, R. Issa, A hybrid continuum/PDF model for the prediction of dispersed particulate flow, International Journal of Multiphase Flow 39 (2012) 148–158.

[108] A. Vié, H. Pouransari, R. Zamansky, A. Mani, Particle-laden flows forced by the disperse phase: Comparison between Lagrangian and Eulerian simulations, International Journal of Multiphase Flow 79 (2016) 144–158.

[109] V. Alopaeus, M. Laakkonen, J. Aittamaa, Solution of population balances with breakage and agglomeration by high-order moment-conserving method of classes, Chemical Engineering Science 61 (2006) 6732–6752.

[110] J. Kumar, M. Peglow, G. Warnecke, S. Heinrich, L. Mörl, Improved accuracy and convergence of discretized population balance for aggregation: The cell average technique, Chemical Engineering Science 61 (2006) 3327–3342.

[111] Q. Li, J. Cheng, C. Yang, Z. Mao, CFD-PBE simulation of a bubble column by the cell average method, Chemical Engineering & Technology (2017) In Press.

[112] M. Yu, J. Lin, T. Chan, A new moment method for solving the coagulation equation for particles in Brownian motion, Aerosol Science and Technology 42 (2008) 705–713.

[113] M. Yu, J. Lin, Nanoparticle-laden flows via moment method: a review, International Journal of Multiphase Flow 36 (2010) 144–151.

[114] J. Lin, Z. Yin, F. Gan, M. Yu, Penetration efficiency and distribution of aerosol particles in turbulent pipe flow undergoing coagulation and breakage, International Journal of Multiphase Flow 61 (2014) 28–36.

[115] T. Chan, S. Liu, Y. Yue, Nanoparticle formation and growth in turbulent flows using the bimodal TEMOM, Powder Technology 323 (2017) 507–517.

[116] M. Strumendo, H. Arastoopour, Solution of bivariate population balance equations using the finite size domain complete set of trial functions method of moments (FCMOM), Industrial & Engineering Chemistry Research 48 (2008) 262–273.

[117] E. Abbasi, H. Arastoopour, Numerical analysis and implementation of finite domain complete trial functions method of moments (FCMOM) in CFD codes, Chemical Engineering Science 102 (2013) 432–441.

[118] S. Wu, E. Yapp, J. Akroyd, S. Mosbach, R. Xu, W. Yang, M. Kraft, A moment projection method for population balance dynamics with a shrinkage term, Journal of Computational Physics 330 (2017) 960–980.

[119] S. Wu, E. Yapp, J. Akroyd, S. Mosbach, R. Xu, W. Yang, M. Kraft, Extension of moment projection method to the fragmentation process, Journal of Computational Physics 335 (2017) 516–534.

[120] J. Cheng, R. Fox, Kinetic modeling of nanoprecipitation using CFD coupled with a population balance, Industrial & Engineering Chemistry Research 49 (2010) 10651–10662.

[121] R. McGraw, Description of aerosol dynamics by the quadrature method of moments, Aerosol Science and Technology 27 (1997) 255–265.

[122] R. Gordon, Error bounds in equilibrium statistical mechanics, Journal of Mathematical Physics 9 (1968) 655–663.

[123] J. Wheeler, Modified moments and gaussian quadratures, The Rocky Mountain Journal of Mathematics 4 (1974) 287–296.

[124] J. Barrett, N. Webb, A comparison of some approximate methods for solving the aerosol general dynamic equation, Journal of Aerosol Science 29 (1998) 31–39.

[125] D. Marchisio, J. Pikturna, R. Fox, R. Vigil, A. Barresi, Quadrature method of moments for population-balance equations, AIChE Journal 49 (2003) 1266–1276.

[126] D. Marchisio, R. Vigil, R. Fox, Quadrature method of moments for aggregation–breakage processes, Journal of Colloid and Interface Science 258 (2003) 322–334.

[127] D. Marchisio, R. Fox, Solution of population balance equations using the direct quadrature method of moments, Journal of Aerosol Science 36 (2005) 43–73.

[128] C. Yuan, R. Fox, Conditional quadrature method of moments for kinetic equations, Journal of Computational Physics 230 (2011) 8216–8246.

[129] C. Yuan, F. Laurent, R. Fox, An extended quadrature method of moments for population balance equations, Journal of Aerosol Science 51 (2012) 1–23.

[130] M. Attarakih, Integral formulation of the population balance equation: Application to particulate systems with particle growth, Computers & Chemical Engineering 48 (2013) 1–13.

[131] J. Su, Z. Gu, Y. Li, S. Feng, X. Xu, An adaptive direct quadrature method of moment for population balance equations, AIChE Journal 54 (2008) 2872–2887.

[132] R. Fox, F. Laurent, A. Vié, Conditional hyperbolic quadrature method of moments for kinetic equations, Journal of Computational Physics Submitted (2017).

[133] M. Attarakih, C. Drumm, H. Bart, Solution of the population balance equation using the sectional quadrature method of moments (SQMOM), Chemical Engineering Science 64 (2009) 742–752.

[134] M. Attarakih, M. Jaradat, C. Drumm, H. Bart, S. Tiwari, V. Sharma, J. Kuhnert, A. Klar, Solution of the population balance equation using the one primary and one secondary particle method (OPOSPM), Computer Aided Chemical Engineering 26 (2009) 1333–1338.

[135] M. Jaradat, M. Attarakih, H. Bart, RDC extraction column simulation using the multi-primary one secondary particle method: Coupled hydrodynamics and mass transfer, Computers & Chemical Engineering 37 (2012) 22–32.

[136] Z. Chen, J. Lin, M. Yu, A direct expansion method of moments for Brownian coagulation, Physica Scripta 89 (2014) 125–204.

[137] M. Yu, J. Lin, J. Cao, M. Seipenbusch, An analytical solution for the population balance equation using a moment method, Particuology 18 (2015) 194–200.

[138] M. Frenklach, Method of moments with interpolative closure, Chemical Engineering Science 57 (2002) 2229–2239.

[139] S. Lo, P. Rao, Modelling of droplet breakup and coalescence in an oil-water pipeline, in: 6th International Conference on Multiphase Flow, ICMF 2007, 2007.

[140] D. Wright, R. McGraw, D. Rosner, Bivariate extension of the quadrature method of moments for modeling simultaneous coagulation and sintering of particle populations, Journal of Colloid and Interface Science 236 (2001) 242–251.

[141] C. Yoon, R. McGraw, Representation of generally mixed multivariate aerosols by the quadrature method of moments: I. Statistical foundation, Journal of Aerosol Science 35 (2004) 561–576.

[142] J. Bałdyga, G. Tyl, M. Bouaifi, Application of gaussian cubature to model two-dimensional population balances, Chemical and Process Engineering 38 (2017) 393–409.

[143] L. Metzger, M. Kind, The influence of mixing on fast precipitation processes–A coupled 3D CFD-PBE approach using the direct quadrature method of moments (DQMOM), Chemical Engineering Science 169 (2017) 284–298.

[144] A. Liné, C. Frances, Discussion on DQMOM to solve a bivariate population balance equation applied to a grinding process, Powder Technology 295 (2016) 234–244.

[145] T. Kim, Y. Kim, DQMOM approach for poly-dispersed soot formation processes in a turbulent non-premixed ethylene/air flame, Chemical Engineering Science 152 (2016) 426–435.

[146] X. Duan, X. Feng, C. Yang, Z. Mao, CFD modeling of turbulent reacting flow in a semi-batch stirred-tank reactor, Chinese Journal of Chemical Engineering (2017) In Press.

[147] K. Jareteg, S. Sasic, P. Vinai, C. Demazière, A numerical framework for bubble transport in a subcooled fluid flow, Journal of Computational Physics 345 (2017) 373–403.

[148] C. Chalons, R. Fox, M. Massot, A multi-Gaussian quadrature method of moments for gas-particle flows in a LES framework, in: Studying Turbulence Using Numerical Simulation Databases, Center for Turbulence Research, Summer Program 2010, Stanford University, 2010.

[149] G. Williams, Combustion theory, Addison-Wesley, 1985.

[150] S. Friedlander, D. Smoke, Haze: Fundamentals of aerosol dynamics, Oxford University Press, New York (2000).

[151] M. Seiler, F. Seiler, Numerical recipes in C: the art of scientific computing, Risk Analysis 9 (1989) 415–416.

[152] S. Kumar, D. Ramkrishna, On the solution of population balance equations by discretization–I. A fixed pivot technique, Chemical Engineering Science 51 (1996) 1311–1332.

[153] C. Peña-Monferrer, A. Passalacqua, S. Chiva, J. Muñoz-Cobo, CFD modelling and validation of upward bubbly flow in an adiabatic vertical pipe using the quadrature method of moments, Nuclear Engineering and Design 301 (2016) 320–332.

[154] L. Silva, R. Damian, P. Lage, Implementation and analysis of numerical solution of the population balance equation in CFD packages, Computers and Chemical Engineering 32 (2008) 2933–2945.

[155] R. McGraw, D. Wright, Chemically resolved aerosol dynamics for internal mixtures by the quadrature method of moments, Journal of Aerosol Science 34 (2003) 189–209.

[156] M. Pollack, S. Salenbauch, D. Marchisio, C. Hasse, Bivariate extensions of the Extended Quadrature Method of Moments (EQMOM) to describe coupled droplet evaporation and heat-up, Journal of Aerosol Science 92 (2016) 53–69.

[157] R. Fan, D. Marchisio, R. Fox, Application of the direct quadrature method of moments to polydisperse gas–solid fluidized beds, Powder Technology 139 (2004) 7–20.

[158] A. Buffo, M. Vanni, D. Marchisio, Multidimensional population balance model for the simulation of turbulent gas–liquid systems in stirred tank reactors, Chemical Engineering Science 70 (2012) 31–44.

[159] K. Swiderski, D. Caviezel, M. Labois, D. Lakehal, C. Narayanan, Computational modelling of gas–liquid multiphase flows with DQMOM and the N-phase Algebraic Slip Model, Computational Methods in Multiphase Flow VIII 89 (2015) 299–310.

[160] N. Lebaz, A. Cockx, M. Spérandio, A. Liné, J. Morchain, Application of the Direct Quadrature Method of Moments for the modelling of the enzymatic hydrolysis of cellulose: II. Case of insoluble substrate, Chemical Engineering Science 149 (2016) 322–333.

[161] N. Lebaz, A. Cockx, M. Spérandio, A. Liné, J. Morchain, Application of the Direct Quadrature Method of Moments for the modelling of the enzymatic hydrolysis of cellulose: I. Case of soluble substrate, Chemical Engineering Science 149 (2016) 306–321.

[162] S. Singer, Direct Quadrature Method of Moments with delumping for modeling multicomponent droplet vaporization, International Journal of Heat and Mass Transfer 103 (2016) 940–954.

[163] L. Sun, W. Yu, M. Hassan, S. Wang, G. Liu, H. Lu, Investigation of aggregation kernel and simulation of cohesive particle flow, Chemical Engineering & Technology 39 (2016) 1858–1866.

[164] H. Zhang, Z. Wang, W. Song, S. Li, Simulation of fine polydisperse particle condensational growth under an octadecane–nitrogen atmosphere, Particuology (2017) In Press.

[165] E. Madadi-Kandjani, A. Passalacqua, An extended quadrature-based moment method with log-normal kernel density functions, Chemical Engineering Science 131 (2015) 323–339.

[166] A. Vié, C. Chalons, R. Fox, F. Laurent, M. Massot, A multi-Gaussian quadrature method of moments for simulating high stokes number turbulent two-phase flows, Center for Turbulence Research Annual Research Briefs 2011 (2011) 309.

[167] A. Vié, F. Laurent, M. Massot, Size-velocity correlations in hybrid high order moment/multi-fluid methods for polydisperse evaporating sprays: Modeling and numerical issues, Journal of Computational Physics 237 (2013) 177–210.

[168] X. Hu, A. Passalacqua, R. Fox, Application of quadrature-based uncertainty quantification to the NETL small-scale challenge problem SSCP-I, Powder Technology 272 (2015) 100–112.

[169] M. Pigou, J. Morchain, P. Fede, M. Penet, G. Laronze, An assessment of methods of moments for the simulation of population dynamics in large-scale bioreactors, Chemical Engineering Science 171 (2017) 218–232.

[170] A. Wick, T. Nguyen, F. Laurent, R. Fox, H. Pitsch, Modeling soot oxidation with the Extended Quadrature Method of Moments, Proceedings of the Combustion Institute 36 (2017) 789–797.

[171] C. Chalons, R. Fox, F. Laurent, M. Massot, A. Vié, Multivariate gaussian extended quadrature method of moments for turbulent disperse multiphase flow, Multiscale Modeling & Simulation 15 (2017) 1553–1583.
[172] E. Madadi-Kandjani, R. Fox, A. Passalacqua, Application of the Fokker-Planck molecular mixing model to turbulent scalar mixing using moment methods, Physics of Fluids 29 (2017) 065–109.
[173] A. Dale, G. Lowry, E. Casman, Accurate and fast numerical algorithms for tracking particle size distributions during nanoparticle aggregation and dissolution, Environmental Science: Nano 4 (2017) 89–104.
[174] M. Petitti, M. Vanni, D. Marchisio, A. Buffo, F. Podenzani, Simulation of coalescence, break-up and mass transfer in a gas–liquid stirred tank with CQMOM, Chemical Engineering Journal 228 (2013) 1182–1194.
[175] A. Buffo, D. Marchisio, M. Vanni, P. Renze, Simulation of polydisperse multiphase systems using population balances and example application to bubbly flows, Chemical Engineering Research and Design 91 (2013) 1859–1875.
[176] S. Salenbauch, A. Cuoci, A. Frassoldati, C. Saggese, T. Faravelli, C. Hasse, Modeling soot formation in premixed flames using an extended conditional quadrature method of moments, Combustion and Flame 162 (2015) 2529–2543.
[177] D. Dunn, K. Squires, Modeling dilute gas–solid flows using a polykinetic moment method approach, Journal of Fluids Engineering 138 (2016) 1–12.
[178] C. Chalons, D. Kah, M. Massot, Beyond pressureless gas dynamics: quadrature-based velocity moment models, arXiv preprint arXiv:1011.2974 (2010).
[179] A. Passalacqua, F. Laurent, E. Madadi-Kandjani, J. Heylmun, R. Fox, An open-source quadrature-based population balance solver for openfoam, Chemical Engineering Science 176 (2018) 306–318.
[180] G. Boccardo, D. Marchisio, R. Sethi, Microscale simulation of particle deposition in porous media, Journal of colloid and interface science 417 (2014) 227–237.
[181] D. Drew, Mathematical modeling of two–phase flow, Annual Review of Fluid Mechanics 15 (1982) 261–291.
[182] M. Ishii, K. Mishima, Two-fluid model and hydrodynamic constitutive relations, Nuclear Engineering and Design 82 (1984) 107–126.
[183] M. Lopez De Bertodano, W. Fullmer, A. Clausse, V. Ransom, Two-Fluid Model Stability, Simulation and Chaos, Springer, 2016.
[184] P. Oliveira, R. Issa, Numerical aspects of an algorithm for the Eulerian simulation of two-phase flows, International Journal for Numerical Methods in Fluids 43 (2003) 1177–1198.
[185] H. Weller, Derivation, modelling and solution of the conditionally averaged two-phase flow equations, Nabla Ltd, Technical Report TR/HGW/02 (2002).
[186] A. Buffo, M. Vanni, D. Marchisio, On the implementation of moment transport equations in OpenFOAM: Boundedness and realizability, International Journal of Multiphase Flow 85 (2016) 223–235.
[187] J. Boris, D. Book, Flux-corrected transport. I. SHASTA, a fluid transport algorithm that works, Journal of computational physics 11 (1973) 38–69.
[188] J. Ferziger, M. Peric, Computational methods for fluid dynamics, Springer Science & Business Media, 2012.
[189] D. Wright, Numerical advection of moments of the particle size distribution in eulerian models, Journal of Aerosol Science 38 (2007) 352–369.
[190] L. Mazzei, D. Marchisio, P. Lettieri, New quadrature-based moment method for the mixing of inert polydisperse fluidized powders in commercial CFD codes, AIChE Journal 58 (2012) 3054–3069.
[191] V. Vikas, Z. Wang, R. Fox, Realizable high-order finite-volume schemes for quadrature-based moment methods applied to diffusion population balance equations, Journal of Computational Physics 249 (2013) 162–179.
[192] F. Laurent, T. Nguyen, Realizable second-order finite-volume schemes for the advection of moment sets of the particle size distribution, Journal of Computational Physics 337 (2017) 309–338.
[193] J. Shohat, J. Tamarkin, The problem of moments, no. 1, American Mathematical Soc., 1943.
[194] V. Vikas, Z. Wang, A. Passalacqua, R. Fox, Realizable high-order finite-volume schemes for quadrature-based moment methods, Journal of Computational Physics 230 (2011) 5328–5352.
[195] W. Gautschi, Orthogonal polynomials: computation and approximation, Oxford University Press on Demand, 2004.
[196] M. Attarakih, H. Bart, N. Faqir, Numerical solution of the bivariate population balance equation for the interacting hydrodynamics and mass transfer in liquid–liquid extraction columns, Chemical Engineering Science 61 (2006) 113–123.
[197] J. Bałdyga, W. Orciuch, Barium sulphate precipitation in a pipe—an experimental study and CFD modelling, Chemical Engineering Science 56 (2001) 2435–2444.
[198] R. Oertel, D. Li, M. Pollack, S. Saalenbauch, C. Hasse, D. Lucas, Population balance modeling using class and quadrature-based moment methods with application to bubbly flows, in: 5th OpenFOAM User Conference, 2017.
[199] D. Li, Z. Li, Z. Gao, Quadrature-based moment methods for the population balance equation: An algorithm review, Chinese Journal of Chemical Engineering 27 (2019) 483–500.